TRIBHUVAN UNIVERSITY
INSTITUTE OF ENGINEERING
PULCHOWK CAMPUS

B-04-BAS-2018/23

INVESTIGATION OF CRACK PROPAGATION ON A THIN PLATE WITH AN IMPLEMENTATION OF PHASE-FIELD

SUBMITTED BY

Amit Kumar Gupta (075AER004)
Helina Khanal (075AER015)
Shrawan Tamrakar (075AER041)

A PROJECT REPORT
SUBMITTED TO THE DEPARTMENT OF MECHANICAL AND AEROSPACE ENGINEERING
IN PARTIAL FULFILLMENT OF THE REQUIREMENTS FOR THE DEGREE OF BACHELOR IN AEROSPACE ENGINEERING

DEPARTMENT OF MECHANICAL AND AEROSPACE ENGINEERING
LALITPUR, NEPAL

MARCH, 2023

COPYRIGHT

TRIBHUVAN UNIVERSITY

INSTITUTE OF ENGINEERING

PULCHOWK CAMPUS

DEPARTMENT OF MECHANICAL AND AEROSPACE ENGINEERING

The undersigned certify that they have read, and recommended to the Institute of Engineering for acceptance, a project report entitled "Investigation of crack propagation on a thin plate with an implementation of phase-field" submitted by Amit Kumar Gupta, Helina Khanal, and Shrawan Tamrakar in partial fulfillment of the requirements for the degree of Bachelor of Aerospace Engineering.

_____

Supervisor, Kamal Darlami
Assistant Professor
Department of Mechanical and Aerospace Engineering

_____

Supervisor, Aayush Bhattarai
Assistant Professor
Department of Mechanical and Aerospace Engineering

_____

External Supervisor, Spad Acharya
Lecturer
Sagarmatha Engineering College

_____

Committee Chairperson
Assoc. Prof. Dr. Surya Prasad Adhikari
Head, Department of Mechanical and Aerospace Engineering

_____

Date

ABSTRACT

Phase-Field Model is an innovative approach for the simulation of crack propagation in the material. Instead of the traditional method of re-meshing and tracking the crack's tip, the phase-field model is based on the principle of minimum energy and uses a continuous phase-field variable to separate the crack from the matrix. This project utilizes the phase-field problem to solve for the minimum elastic energy by combining two functions, the phase-field parameter, and mechanical displacement, over a defined area domain for an anti-plane elastic solid. The governing equation is solved using PDE models and FEM methods in MATLAB's PDE Toolbox. The results of the study demonstrate the advantages of the phase-field model in predicting the effects of varying shear modulus and notch location and geometry on crack propagation in anti-plane elastic solids. To further validate the effectiveness of the code, notched specimens were tested with tension loading in the UTM and compared with simulation results, advertising the phase-field model's real-world applications for failure prediction.

Keywords*: Phase-Field Model, Crack Propagation, Phase-Field Parameter, MATLAB*

ACKNOWLEDGEMENT

We would like to express our deepest appreciation to the Department of Mechanical and Aerospace Engineering of Pulchowk Campus for allowing us to take on a final-year project.

We are highly indebted to our supervisors Asst. Prof. Kamal Darlami and Asst. Prof. Aayush Bhattarai for his continuous guidance, motivation, and assistance in carrying out this project. We are sincerely thankful to Asst. Prof. Sudip Bhattarai for their valuable suggestions and assistance. We are also grateful to Mr. Chhedi Narayan Sharma for helping us with UTM testing.

Furthermore, we would like to thank our friends, family, and other personnel who supported and helped us throughout the project. We would also like to take this opportunity to appreciate the crucial role of various journals and research papers in providing us with the required information.

TABLE OF CONTENTS

LIST OF TABLES

LIST OF FIGURES

LIST OF SYMBOLS

φ	Order parameter
u	Displacement field
v	Phase-field
Ω	Region occupied by the body
W	Strain energy density
κ	Regularization parameter/ Length-scale parameter
μ	Modulus of rigidity
u_z	Displacement in z-direction
a	Regularization coefficient
c	Regularization coefficient
f	Forcing or source function
K	Stress intensity function
G_c	Critical energy release rate
G	Energy release rate
π	Potential energy
s	Surface of fracture
S_t	Surface of the body
τ	Tensile load
b	Body force
γ	Surface energy
U_f	Inelastic energy dissipation per unit of crack growth
ε	Strain
$\mathbb{C}$	Stiffness tensor
ϵ	Length-scale parameter
η	Residual stiffness
h	Mesh step

LIST OF ABBREVIATIONS

2D	Two Dimensional
3D	Three Dimensional
DECSG	Decompose Constructive Solid Geometry
FEM	Finite Element Method
GB	Gigabytes
GFEM	Generalized Finite Element Method
Gpa	Giga Pascal
KKL Model	Karma, Kessler, Levine model
MATLAB	Matrix Laboratory
Mpa	Mega Pascal
Msi	Mega-pounds per square inch
OS	Operating System
PDE	Partial Differential Equation
PFM	Phase-Field Model
RAM	Random Access Memory
S/m	Siemens per meter
UTM	Universal Testing Machine
W/mK	Weber per meter Kelvin
XFEM	Extended Finite Element Method

CHAPTER ONE: INTRODUCTION

1.1 Background

1.1.1 Introduction to Phase-Field Model

Phase-Field Model (PFM) is a mathematical method for modeling the behavior of materials that undergo phase transitions, such as solidification, crystallization, or microstructural evolution. It works by dividing the material into small regions, or phases, and using partial differential equations to describe how the boundary between these phases changes over time. PFM can be used for the simulation of complicated fracture processes such as crack initiation, propagation, coalescence, and branching. The simulation for fracture evaluation can be done on a fixed mesh. The phase-field method employs a single variable, referred to as the order parameter φ, to continuously represent the state of the complete microstructure. For example, φ = 0 and φ = 1 represent cracks and non-cracks respectively in the material. Order parameters simply are field variables that remain constant in bulk and their changes indicate the presence of an interface.

The phase-field model uses a scalar order parameter to represent fracture and material parameters to simulate changes in the stiffness of damaged and undamaged materials. For undamaged material, the value of the order parameter is 1, and there is no effect on the property of the material. On the other hand, the value of zero represents the broken material, and this results in a corresponding reduction in stiffness. As a result, the phase-field model depicts cracks as lines or regions in the material where the value of the order parameter is zero, and the stiffness is significantly decreased. The advantage of this approach is that cracks don't have to be treated as material boundaries, which is particularly useful when implementing the fracture model using finite element methods.

Typically, a phase-field model is designed to capture the correct behavior of interfacial dynamics in the sharp interface limit, which involves an infinitesimal interface width. This allows the problem to be solved by the integration of a set of partial differential equations for the entire system, without requiring definite treatment of boundary conditions at the interface. The concept of phase-field models was propounded by Fix and Langer.

1.1.2 Need for Phase-Field Model

Material failure is a critical aspect of engineering, and various numerical methods have been developed to deal with fracture problems. These methods are broadly categorized into two types: continuous and discontinuous approaches.

Discontinuous approaches such as XFEM and GFEM introduce strong discontinuities in the displacement field. This approach discretizes the material into small elements, and the displacement field is represented as a piecewise polynomial function. The discontinuous approach and its accuracy are highly dependent on the mesh, and the mesh must be refined near the crack tip to capture the behavior of the material accurately. All these aspects make the approach complex, tedious, and time-consuming.

In contrast, continuous methods such as the Phase-Field Model (PFM) avoid introducing discontinuities in the displacement field. Instead, the evolution equation of the phase-field is used to describe fracture propagation. This involves using a scalar field (phase-field) to represent the crack in a diffusive manner. The PFM approach doesn't require continuous mesh refinement, and a single equation governs the entire process. Moreover, the PFM offers great flexibility in selecting boundary conditions, enabling the modeling of different types of loading conditions such as homogeneous and inhomogeneous boundary conditions. All of these factors indicate the significance of introducing the PFM for the analysis of fractures.

1.1.3 Application of Phase-Field Model

The techniques of the phase-field model can be used extensively in engineering as well as material science mainly to evaluate phase boundaries and materials that go through phase transformation. Phase-Field Model can be used in microstructure evolution such as solidification, grain growth and coarsening, domain evolution in thin films, pattern formation on surfaces, solid-state structural phase transformations, dislocation microstructures, and crack propagation. The model deals with energies leading to phase transformations, and their minimization and describes the change with the help of order parameters. For the study of crack propagation, there are two phases: solid and broken. These phases are represented as 1 and 0 by an order parameter.

1.1.4 Crack in Metals

When a crack grows in a material, it generates new surfaces that act as the faces of the crack. This process demands energy to overcome the cohesive force at increasing surface energy. Griffith came up with a principle for crack propagation by analyzing the balance of energy using these two types of energies. According to his principle, a crack can propagate only when the reduction in elastic strain energy is equal to or greater than the energy needed to create the new surface caused by the crack growth. The extent of the tensile stress needed to propagate a brittle fracture and a crack of a particular size is determined by the thermodynamic connection between these two forms of energy.

1.1.5 Crack Propagation in Brittle Fracture

The propagation of cracks in a material is a result of energy derived from various factors, including mechanical, thermal, and chemical effects. These factors, either individually or in combination, can affect crack initiation and growth. Crack propagation in a brittle fracture occurs in several steps leading to final failure. The major steps for crack propagation in brittle fracture can be summarized as follows:

i. Elastic deformation: In this step, the deformation material is directly proportional to the applied tensile load. The process of elastic deformation occurs up to maximum load. The process can be seen in the initial portion of the force vs displacement graph.

ii. Crack initiation: In case of brittle fracture, the process of crack initiation occurs when there is a pre-existing defect in the material. The process occurs when the applied tensile load exceeds the strength of the material.

iii. Formation of microcracks: Before the starting of crack propagation, microcracks will form at the point of high-stress concentration. The point of high-stress concentration is at the tip of the notch and such point, the microcracks are formed even at relatively low stress.

iv. Crack propagation: After the formation of microcracks, the propagation of the crack will be rapid without significant plastic deformation. The crack will continue till it reaches a critical length.

v. Failure: After the crack reaches a critical length, the material is not able to withstand applied load leading to failure.

1.1.6 Phase-Field Model for Crack Propagation

The Phase-Field Model (PFM) represents fracture as a continuous field, referred to as the phase-field. The term ‘phase-field’ is a scalar function that ranges from 0 to 1, with 0 indicating a region completely fractured and 1 indicating a region with no cracks. A set of partial differential equations are used to describe the changes in the phase-field over time and these equations model the development of the crack. PFM can monitor the crack growth process without explicitly requiring the monitoring of the crack tip, eliminating the need for mesh refinement near the fracture tip. The value order parameter varies steadily between the values given to the different phases of the material at interfaces where broken and unbroken materials meet. The regularization parameter determines the size of the transition zone that encloses the phase-field cracks. It can be shown that for the phase-field fracture model, the underlying energy expressions in the limit of a dissipating regularization length converge to the surface and elastic energy of Griffith's formulation. Thus, Griffith's fracture criterion can be regularized by the phase-field fracture model. Furthermore, the phase-field model can be used to simulate complicated fracture geometries, such as branched cracks or cracks that interact with other microstructural characteristics.

1.1.6.1 Governing Equations

To simulate crack propagation using the phase-field model, an equation that governs the crack's propagation based on energies is needed. The equation is derived from Griffith's theory, and in the case of a thin plate with uniform thickness, a straight initial crack, and subject to displacement at one of its edges, its behavior is analyzed. The main consideration is the thin plate under tension obeying Hooke's law. The governing equation comes from the variational approach of brittle fracture based on regularization formulation. The energy function in equation (1.1) is the sum of both elastic energy due to displacement and fracture energy due to crack, and the minimization of this energy function governs crack initiation, propagation, and branching. As the applied load increases, the crack initiates and propagates, converting the elastic energy into fracture energy. The governing energy equation is:

$$\mathrm{E}\,(u,v) = \int_{\Omega} v^2 W(\nabla u)\, d\Omega + \int_{\Omega} \left[\frac{(1-v)^2}{4\kappa} + \kappa |\nabla v|^2 \right] d\Omega \tag{1.1}$$

Here, the first term represents the elastic energy whereas the second term represents the fracture energy. The displacement field is represented by *u* and the phase-field is represented by *v*. The scalar field *v* varies continuously between *v=1* (intact material) and *v=0* (fully damaged material). The term $W(\nabla u)$ known as the elastic energy density is represented as:

$$W\,(\nabla u) = \int_{\Omega} \frac{\mu}{2} |\nabla u_z|^2\, d\Omega \tag{1.2}$$

Where μ is the modulus of rigidity of the brittle material. The parameter κ has the dimension of a length that controls the transition zone between the completely damaged and intact body. The governing equation is minimized and further solved to get the partial differential equations for obtaining displacement field u and phase-field v. The partial differential equation is the elliptic type. The partial differential equations are solved within the framework of the FEM using the MATLAB PDE toolbox. The partial differential equation expected by the MATLAB PDE toolbox is:

$$au - c \cdot \nabla^2 u = f \tag{1.3}$$

The above equation describes the behavior of *u*, where ∇^2 represents the Laplacian operator, which calculates the second spatial derivative of *u*. The term '*au*' represents the rate of change of *u* in time, and the term 'c ∇^2u' represents the rate of change of *u* in space. The term '*f*' is a source or forcing function that drives the change in *u*. The parameters *a, c,* and *f* are assigned properly. Respectively the behavior of *v* is described in the same way as assigning the values of *a, c,* and *f* properly.

1.1.6.2 Elliptical PDE and its Features

An elliptic partial differential equation (PDE) is a type of PDE that describes a wide range of physical phenomena including fracture phenomenon and elasticity. The various key features of elliptic PDEs include:

i. Second-order derivatives: Elliptic PDEs uses second-order partial derivatives of the unknown function. This is in contrast to hyperbolic and parabolic PDEs, which involve first and second-order derivatives, respectively.

ii. Constant coefficients: The coefficients of the second-order derivatives are constant. This means that the PDE is homogeneous, and its solutions are invariant under translations and rotations.

iii. Positive-definite: The coefficient matrix of the second-order derivatives is positive-definite. This ensures that the PDE has a unique solution, and it also ensures that the solutions are smooth and have no sharp corners or edges.

iv. Boundary conditions: Elliptic PDEs are typically solved subject to boundary conditions, which specify the values of the unknown function on the boundary of the domain. These boundary conditions can be Dirichlet (prescribing the value of the function), Neumann (prescribing the normal derivative of the function), or mixed (prescribing a combination of the value and normal derivative).

v. Laplace's equation: The most famous example of an elliptic PDE is Laplace's equation, which describes the steady-state distribution of a scalar field in a region with no sources or sinks. Laplace's equation is a homogeneous PDE, and its solutions are harmonic functions.

vi. Maximum principle: Elliptic PDEs satisfy the maximum principle, which states that the maximum and minimum values of the solution occur on the boundary of the domain. This property is useful for proving the uniqueness of solutions and for obtaining qualitative information about the behavior of solutions.

vii. Sobolev spaces: The solutions of elliptic PDEs typically belong to the Sobolev space, which is a function space that captures the regularity and smoothness of the solutions. The Sobolev space provides a natural framework for studying the existence and regularity of solutions.

viii. Numerical methods: Numerical methods for solving elliptic PDEs include finite difference, finite element, and spectral methods. These methods are widely used in engineering and scientific applications, and they require careful analysis to ensure their accuracy and convergence.

ix. Variational formulation: Elliptic PDEs can be formulated as variational problems, which involve minimizing a function over a function space subject to certain constraints. This approach provides a powerful tool for solving PDEs and for obtaining qualitative information about their solutions.

1.1.6.3 Shear Modulus

The modulus of rigidity or shear modulus is a mechanical characteristic of a material that represents its ability to resist shear deformation. It quantifies a material's rigidity when subjected to shear stress and is one of the fundamental elastic moduli, alongside Young's modulus and Poisson's ratio. The shear modulus can be defined as the ratio of shear stress to shear strain within a material and is mathematically expressed as the derivative of shear stress concerning shear strain. Typically, the shear modulus is measured in units of gigapascals *(GPa)* or mega-pounds per square inch *(Msi)*. The shear modulus is a crucial parameter in the analysis of metal structures as it provides essential information about the material's ability to resist deformation and stiffness.

1.1.6.4 Elastic and Fracture Energy

The elastic energy of a material is a quantity that represents the energy that is stored within the material as a result of deformation due to the application of stress. Deformation refers to the change in shape experienced by metal when subjected to stress. The energy required to cause this deformation is stored within the material as elastic energy.

Fracture energy is a crucial factor in the field of fracture mechanics that indicates the amount of energy necessary to initiate and advance a crack in a metal. It is a valuable parameter in evaluating the durability and crack resistance of a material. Essentially, fracture energy is the amount of energy needed to produce a new surface area when a crack advances through the material. As the crack propagates, the material stores the energy as strain energy, which is eventually released.

1.1.6.5 Anti-plane Solid

Anti-plane solids refer to solid objects or materials designed to resist deformation in a single plane, typically perpendicular to the loading plane. This means that the material can resist forces that would cause it to bend or deform in one direction while remaining flexible in other directions. In anti-plane deformation, the displacement along the plane of constant displacement is accompanied by a change in the shape of the solid and its volume change. The behavior of anti-plane solids is governed by equations that describe the mechanical behavior of the solid, such as its elasticity, strength, and stress-strain relationship. These equations are used to predict the response of the solid to external loads and to design structures that are capable of resisting these loads.

1.1.6.6 Staggered Scheme

In the context of the phase-field model, the staggered scheme is a numerical scheme used to solve the partial differential equations that govern the evolution of the phase-field variable. The staggered scheme involves discretizing the spatial domain into a grid, where the values of the phase-field variable are defined at the center of the grid cells, while the values of other variables like potential energy are defined at the edges of the grid cells.

The staggered scheme involves the following steps:

i. Discretize the spatial domain into a grid of points with uniform grid spacing.

ii. Offset the order parameter and potential energy grids by half a grid spacing.

iii. Calculate the potential energy on the staggered grid using a finite difference scheme that uses the order parameter on the central grid.

iv. Update the order parameter on the central grid using a finite difference scheme that uses the potential energy on the staggered grid.

v. Repeat steps 3 and 4 for a given time interval until the desired simulation time is reached.

1.1.7 Universal Testing Machine

A UTM is a specialized piece of equipment that tests the mechanical properties of materials by applying tensile, compression, and bending forces to materials and then measures the corresponding deformation and strain. Doing such, a UTM can determine the material's strength, stiffness, ductility, and other mechanical properties of any type of material. UTM is used for experimental validation of our code by applying tension loads on a set test specimen containing notches and measuring the force applied with displacement.

Figure 1.1: UTM setup

Figure 1.2: Computer interface for UTM

A hydraulic UTM typically consists of a frame, a load cell, grips or fixtures to hold the specimen, a hydraulic pump, and a hydraulic cylinder. The specimen is first fixed between the grips to hold it in place, then the hydraulic pump is run so pressure is applied on the hydraulic cylinder, providing force to the workpiece. The load cells measure the force applied and the displacement then sends it to the computer for analysis. Hydraulic UTM has the advantage over mechanical UTMs of giving greater force with higher accuracy and precision.

1.1.8 Mild Steel

Mild Steel is a type of carbon steel with relatively less amount of carbon content, less than 0.3%. When mild steel is subjected to a tensile load, it can develop a crack if the applied stress surpasses the yield strength of the material. This happens because the material stretches in the direction of the load and experiences localized distortion and increased stress levels in areas where it is weak, such as surface defects, notches, or inclusions. If the tensile stress is too high for the material to withstand, plastic deformation may occur and create tiny cracks or voids. With time, these cracks can spread through the material, influenced by cyclic or repeated loading, and result in more severe damage or even failure of the component. The features of mild steel are as follows:

Table 1.1: Properties of Mild Steel

Density	*7850 kg/m^3*
Electrical Conductivity	*3-15% IACS* *6.99 x 10^6 S/m*
Ultimate Tensile Strength	*400 MPa to 550 MPa*
Yield Strength	*250 MPa*
Young's Modulus of Elasticity	*200 GPa*
Thermal Conductivity	*50 W/mK*

1.1.9 PDE Toolbox in MATLAB

The PDE Toolbox is a collection of functions within MATLAB software that enables solving of partial differential equations using numerical methods. The toolbox can handle a range of PDEs, including linear and non-linear, time-dependent, and stationary problems. It is equipped with various numerical methods such as finite element and finite difference methods. Furthermore, it has features that aid in tasks such as mesh generation, which are crucial for solving PDEs using numerical methods. Discretization is also an important feature, which is a crucial step in solving PDEs using numeric methods. The toolbox is also equipped with various post-processing functions for the solutions to PDEs. The solutions can be visualized using contour plots, surface plots, and animations. The wide range of features and support for different types of PDEs available in the PDE toolbox makes it a useful tool for researchers and engineers in various fields.

1.1.10 GUI and App Designer in MATLAB

Graphical User Interface is a method to make a working code more interactive to the user, by using graphical elements such as buttons, sliders, or value editors. Modern computer codes use GUIs regularly to provide a more user-friendly and intuitive experience for the users while using said code. Instead, the users can opt to select an item from menus or only input set variables to perform tasks. This has the advantage of making the code available to a wider audience of users, including those with little to no experience in the programming language. GUIs can also be customized to fit the particular task using specific design elements or layouts to make sure the code is tailored to the specific user needs and preferences.

MATLAB uses App designer as its GUI development environment, which is built into itself as a tool. App designer uses drag-and-drop tools and visual programming techniques to help users in making applications with ease. This tool presents a variety of pre-built components like buttons, sliders, plots, and tables to the user that can be easily arranged and customized to create any desired interface. App designer integrates seamlessly with other MATLAB tools and functions, convenient for use alongside MATLAB’s PDE toolbox.

1.2 Problem Statement

Crack is a primary way that materials fail, and the way cracks propagate can display complex dynamics that depend on both microscopic processes in the crack's tip region and macroscopic elasticity. Detecting cracks and their propagation is challenging, and there are both continuous and discontinuous approaches to the problem. The majority of the research has focused on discontinuous approaches, which create a sharp discontinuity in the displacement field and do not work on a fixed mesh. However, a continuous approach called the Phase-field Model, originally developed for phase transformations, can avoid explicit front tracking by using spatially diffuse material interfaces. This approach can contain the short-scale physics of failure as well as the problems of macroscopic linear elasticity, allowing for simulations on relevant time and length scales. While phase-field models have been applied to various software, there has been limited simulation using the MATLAB platform. The MATLAB toolbox provides several functions for easily and simultaneously solving differential equations.

1.3 Objectives

1.3.1 Main Objective

To investigate crack propagation on a thin plate with an implementation of the Phase-Field Model.

1.3.2 Specific Objectives

i. To implement the phase-field model on a simple geometry.
ii. To study the propagation of cracks in metal.
iii. To develop code in MATLAB.
iv. To compare numerical and experimental data.

1.4 Application

The major applications of our projects are:

i. Prediction of failure
ii. Improvement of manufacturing techniques to minimize risks of failure
iii. Design of material with improved fracture properties

1.5 Features

The major features of our project are:

i. Computational Method
ii. Algorithm and Models
iii. Analysis of Result
iv. Validation of Code and Accuracy

1.6 Feasibility Analysis

1.6.1 Economic Feasibility

The project requires less amount of funding compared to other crack propagation techniques such as XFEM and GFEM. The computational time cost is also relatively low because the need for mesh refinement is eradicated.

1.6.2 Technical Feasibility

The project requires less computational time compared to other techniques. The project can be done using available resources.

1.6.3 Operational Feasibility

The project is practical and feasible to implement and operate. The project can be completed within the available time limit.

1.7 System Requirements

1.7.1 Software Requirements

For the completion of this project, we require MATLAB for coding and simulation. MATLAB R2021a is used for this project.

1.7.2 Hardware Requirements

For the completion of this project, we require a computer that can run MATLAB efficiently. With Windows 10 or higher OS, any 64-bit processor, at least 4 GB of RAM, and up to 35 GB of storage.

For experimental validation, we require a specimen, a setup for UTM, and a camera.

CHAPTER TWO: LITERATURE REVIEW

2.1 Phase-field Model: Development Trends

In engineering and material science, it is crucial to be able to predict when materials, particularly metals, will fail. To address fracture problems, various numerical approaches have been developed, which can mainly be divided into two main categories: continuous and discontinuous approaches [1].

The phase-field model for brittle cracks was first developed in the 1990s and has since generated significant interest among researchers because it can naturally simulate complex fracture processes. The primary advantage of the phase-field model is its capability to simulate the evolution of fracture on a fixed mesh [2].

In case of steel or any other metals, there are two commonly used hypotheses of crack. According to the hypotheses, cracks may occur if (a) the maximum tensile stress or (b) the maximum extension exceeds a certain critical value. According to the traditional theory of minimum energy, "the equilibrium state of an elastic solid body, deformed by specified surface forces, is such that the potential energy of the whole system is minimum". On the contrary, the new theory by Griffith, obtained in addition to traditional ones, suggests that "the equilibrium position, if an equilibrium is possible, must be on in which crack of the solid has occurred if the system can pass from the unbroken to the broken condition by a process involving a continuous decrease in potential energy" [3].

The tip of a crack will start to widen when it reaches a specific critical loading intensity. The critical stress intensity factors, designated as $K_{Ic}, K_{IIc}\ and\ K_{IIIc}$, express the failure criterion and are material parameters dependent on the type of material, its physical characteristics, grain size, strain-hardening, temperature, and pressure levels. Other parameters are also used to describe the criterion of local failure instead of the critical stress intensity factors. If a single parameter can represent such criteria, such as the energy release rate or crack extension force, all criteria can be considered equivalent for linear elastic fracture in the small-scale yielding regime. The energy release rate (G_c) is a commonly used parameter that measures the rate at which the potential energy of the loading system and the elastic strain energy of the material decrease with the extension of the crack [4].

The mechanics community has developed phase-field models for quasi-static fractures using a variational approach to brittle fracture. While Griffith's theory could predict crack growth, it had limitations in predicting crack initiation, its path, and crack jumps along the path. To address these limitations, Francfort and Marigo [5] analyzed a 2-D domain filled with a homogeneous, isotropic, and linearly elastic material with a straight crack. Based on their analysis, they developed the variational approach to fracture, which involved the construction of an energy function which will be able to govern the entire fracture process. By minimizing this energy function the process of crack initiation, propagation, and branching can be obtained [5].

To numerically approximate the variational approach, a two-dimensional body with uniform fracture toughness is subjected to a displacement field. The total energy of the body is calculated, along with three crack conditions. The first condition ensures the crack grows over time. The second condition requires the actual crack to have the lowest total energy compared to all other possible cracks. The third condition tracks previous energy states and can be used to select among all possible crack evolutions [6].

The governing equations in phase-field models are usually seen as partial differential equations, which can be solved using finite element methods (FEM). Therefore, most phase-field approaches are solved using this method. For completely coupled phase-field fracture problems, the space domain is discretized using finite element techniques, and appropriate decoupling methods are applied to solve them [7].

A method for efficiently solving the phase-field model was developed, which involves updating the fracture phase-field and the displacement field incrementally using an operator split algorithm. The algorithm allows for gradual updates of both fields during a time step, and a current history field approximation is used to decouple the linked equations. The approach involves solving two linear problems for updating the phase and displacement fields within a time step, and a staggered plan is suggested as a reliable solution. The method can be used to implement phase-field-type fracture in a rate-independent environment using a conventional framework [8].

FEAP, a Finite Element Analysis Program, now includes the phase-field concept where the phase-field order parameter is considered an extra degree of freedom at each node in addition to the displacement vector. The nodal values within elements can be

interpolated using standard linear shape functions as the formulation of the phase-field which ensures that the displacement and fracture fields remain continuous. An implicit time integration approach is used to discretize the transient evolution equation to ensure stability. The equations for discretized field and the evolution equation form a non-linear coupled system of equations that is solved at each time step using the Newton-Raphson method. The crack field is considered an additional crack indicator rather than a physical crack. To ensure appropriate surface energy recovery upon unloading, boundary conditions with irreversibility restrictions have been selected [9].

The standard phase-field models do not address the issue of premature stiffness degradation around areas of stress concentration, nor do they account for the simulated failure loads' dependence on the regularization parameter. To overcome these limitations, a new set of degradation functions was introduced that is capable of simulating fractures more accurately. The main advantage of these degradation functions is their dependence on a set of parameters that allow for fine-tuning of shapes. The use of a quadratic degradation function also leads to a delay in crack propagation. The new degradation functions can accurately reproduce the start of failure for a broad range of values of the regularization parameter. In cases where the phase-field evolution equation is non-linear, a new linearization scheme that is based on a truncated Taylor series approximation can be used to avoid nested loops in the solution scheme [10].

Simulation of the fracture of solids using computational approaches at the macroscopic scale can be broadly categorized into two types: (a) discrete crack models and (b) smeared crack models. Discrete crack models necessitate the inclusion of discontinuous fields in the numerical model. On the contrary, smeared crack models employ element deletion methods that are based on constitutive laws incorporating strain-softening. Here, a regularized Ambrosio-Tortorelli [11] type model is introduced that includes the impact of unilateral contact and takes into account asymmetric traction and compression behaviors inside a linearized elasticity framework. This approach to fracture prediction is based on the concept of energy density and the classification of strain energy into spherical and deviatoric parts, using the local volume change as a basis. Through the refinement of several numerical aspects, the variational approach to fracture, along with its regularized variations, has become a useful tool for predicting crack paths without requiring any prior assumptions [12].

Order parameters are a more appropriate term to refer to the phase-field variables when modeling cracks. The order parameter creates distinction between the solid phase and the broken phase inside the crack. The transition between these states occurs at the fracture surfaces in the context of the phase-field. In the continuum theory framework, the uniform motion of a crack is comparatively well understood. The typical approach is to represent the crack as a front or interface that divides the broken and unbroken parts of the material, and its propagation is controlled by the equilibrium of the elastic forces in the material and cohesive stresses near the tip of the crack [13].

Crack propagation at low speeds is mainly influenced by macroscopic linear elasticity and traction-free boundary conditions on the fracture surfaces. Thus, simple phenomenological phase-field models, such as the KKL model, can accurately capture the dynamics because the process zone physics does not significantly impact the results. However, for inertial cracks of fast-moving nature, phase-field models reproduce experimentally observed crack branching instabilities. The threshold velocity for branching, which is still not well understood, depends on the process zone description [14].

The researchers utilized Miehe's approach for simulating crack propagation in 2D brittle elastic materials. They studied the behavior of starting horizontal cracks with varying lengths that were located on the horizontal symmetry axis $(y=0.5)$ under pure tension loading. The results showed that an increase in the initial crack length led to a decrease in peak force and maximum displacement, with horizontally symmetric cracks tending to propagate in that direction and displaying similar force-displacement curves for the same initial crack length. Furthermore, the peak force increased as the initial crack moved away from the symmetry axis. The phase-field model based on Miehe's approach was found to be sensitive to the length-scale, including the regularization parameter l and element size h [15].

To simulate crack growth caused by cyclic fatigue, an additional energy contribution is considered, which considers the crack driving forces that are caused by fatigue damage in the regularized energy density function. This energy at the crack surface enables crack extension even under low maximum loads and is a time-dependent elastic strain energy that includes all accumulated energies. The proposed model accurately predicts the growth rates of real-life fatigue cracks and considers the effects of mean stress and various stress ratios [16].

The proposed approach presents a modification to the standard approach to phase-field model for brittle fracture, introducing a distinction between the critical energy release rates for mode-I and mode-II cracks. It has been applied to simulate crack propagation in geotechnical materials, using a new framework based on the division of the fracture energy release rate. The model takes into account that the critical release rate for energy is much lower for tensile fractures than for shear cracks. To address this, the proposed method identifies the energy driving crack propagation and introduces a new degradation function that uses a non-dimensional parameter to describe the different rates of weakening in brittle materials as cracks spread [17].

2.2 Related Theory

2.2.1 Griffith's Theory

The Griffith theory states that, "a crack will propagate when the reduction in potential energy that occurs due to crack growth is greater than or equal to the increase in surface energy due to the creation of new free surfaces."

Griffith's theory can be applied to any elastic material that fracture in brittle fashion. The theory was based on following assumptions:

i. The material is homogeneous, isotropic and brittle.
ii. The crack is sharp having well-defined boundary between two fracture surfaces.
iii. The fracture process is assumed to be quasi-static ignoring effects of inertia and dynamic loading.
iv. The strain energy density is constant throughout the fracture process.

Griffith's theory takes energy release rate G into account which can be defined as the energy that flows over to the tip of crack per unit of new crack surface created. From energy balance:

$$G = \frac{\partial \pi}{\partial s}, \tag{2.1}$$

where s is the surface of fracture and π is the potential energy which is given by,

$$\pi = \int_v W\, dV - \int_{S_t} t \cdot u\, dS - \int_v b \cdot u dV \tag{2.2}$$

where W is the strain energy density, v is the region occupied by a body, S_t is the surface of the body on which tensile (t) is applied, u is the displacement and b is the body force.

The inelastic deformations such as plastic flow, micro cracking and crazing also dissipates energy in the zone surrounding the crack. So, taking the surface energy (γ), and inelastic energy dissipation per unit of crack growth, U_f into consideration, the generalization of Griffith's theory can be given as:

i. The crack grows when the energy released by the body per unit fracture area is greater than or equal to the sum of increase in surface energy and inelastic energy dissipation per unit of crack growth. Mathematically,

$$G \geq 2\gamma + U_f$$

ii. For materials whose $U_f \gg 2\gamma$, the crack criteria is such that the value of energy release rate is greater than or equal to the value of critical energy release rate. Mathematically,

$$G \geq G_c$$

2.3 Overview of Governing Equation

Griffith's theory proposes that crack growth occurs due to the release of strain energy, compensated by additional energy related to the surface area of infinitesimal crack growth. In the phase-field model for brittle fracture, cracks are represented by a continuous transition function *s(x,t)* that varies from 1 for intact material to 0 for broken material. The model uses a regularized equation for brittle fracture, with the goal of minimizing the total internal energy of a loaded and fractured body by determining the displacement and crack patterns represented by *s(x,t)* [10].

$$E = \int_\Omega \psi\,(\varepsilon, s, \nabla s)\, d\Omega = \int_\Omega (g(s) + \eta) W(\varepsilon)\, d\Omega + \Gamma(s, \nabla s)\, d\Omega \tag{2.3}$$

The first term of energy in above equation is the strain energy along with the strain energy density of a linear elastic material

$$W(\varepsilon) = \frac{1}{2}\varepsilon : (\mathbb{C}\varepsilon) \tag{2.4}$$

where $\mathbb{C}$ is the infinitesimal stiffness tensor and ε is the infinitesimal stress tensor. Now, the strains are computed as follows:

$$\varepsilon(u) = \frac{1}{2}(\nabla \mathrm{u} + (\nabla \mathrm{u})^T) \tag{2.5}$$

The second energy term in equation (2.3) is based on Griffith's theory taking crack energy into account which is characterized by the crack energy density

$$\Gamma = G_c \frac{(1-s)^2}{4\epsilon} + \epsilon|\nabla \mathrm{s}|^2 \tag{2.6}$$

where G_c is the critical energy release rate and ϵ is the length scale.

The coefficient is chosen such that the value of η lies between $0 < \eta \ll 1$ so that there is a marginal amount of residual stiffness. This avoids numerical problems concerning the static solution scheme. The most widely used form of a degradation functions is a simple quadratic approach:

$$g(s) = s^2 \tag{2.7}$$

Now, since strain is the change in displacement, from equation (2.4) and equation (2.5) we obtain:

$$W(\nabla u) = \int_\Omega \frac{\mu}{2}(\nabla u_z)^2 \, d\Omega \tag{2.8}$$

Let, Phase-field parameter, s = v

Length scale parameter, $\epsilon = \kappa$

Now, equation (2.6) becomes,

$$\Gamma = G_c \left(\frac{(1-v)^2}{4\kappa} + \kappa|\nabla v|^2 \right) \tag{2.9}$$

The material is taken such that its value of G_c is equal to one which signifies that the toughness of the material is relatively low.

Hence, equation (2.3) becomes,

$$\mathrm{E}\,(u,v) = \int_{\Omega} v^2 W(\nabla u)\, d\Omega + \int_{\Omega} \left[\frac{(1-v)^2}{4\kappa} + \kappa |\nabla v|^2 \right] d\Omega \tag{2.10}$$

2.4 Implementation of MATLAB Code

For variational mode of brittle fracture, the value of critical energy release should be constant. The crack propagation will take place if $G = G_c$, if $G > G_c$ the propagation will be unstable [5]. For simplicity and easiness in computation the value of critical energy rate, G_c=1 [6].

Some of the parameters should be set before computation such as: mesh step 'h' and regularization parameters 'c' and 'κ'.

For the value of regularization parameter 'κ', if κ = 0, the solution to FEM will diverge. On the contrary if the value of 'κ' is very big, some rigidity of the material remains in the cracked region causing bulk energy to be overestimated.

For the value of mesh step 'h', the closer the value of h is to zero that is closer to crack, more refined the mesh becomes. Also, the value for element size must be less than or equals to the half of regularization parameter.

For the value of regularization constant 'c', the value should be small enough to prevent softening effect so that the bulk energy is underestimated. On the contrary, it should be large enough to be compared to discretization steps near crack. Also, the domain must be in accordance to 'c' for accurate estimation of cracks near boundaries [5].

CHAPTER THREE: METHODOLOGY

3.1 Methodology Chart

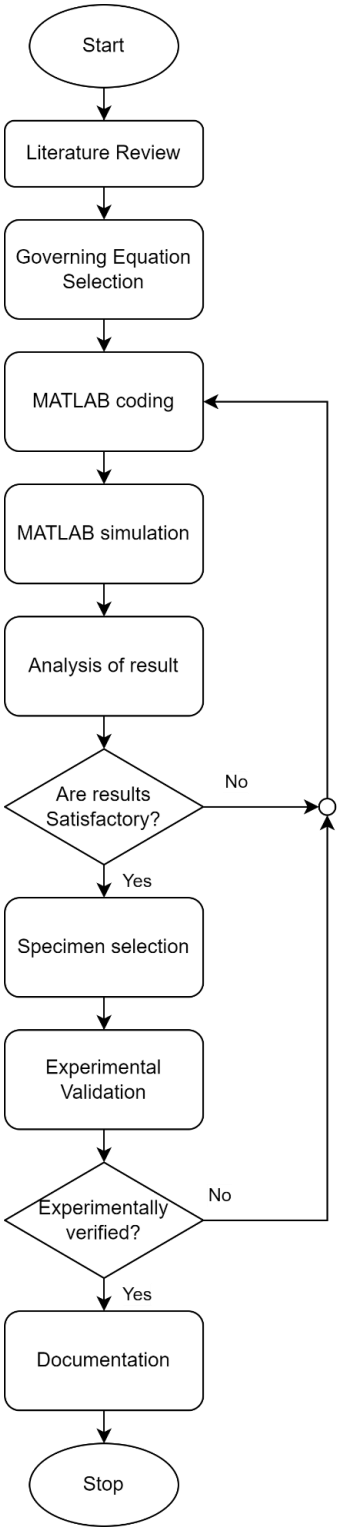

Figure 3.1: Methodology Chart

3.1.1 Governing Equation Selection

The first step in the procedure was to choose the governing equation that can define ductile cracks in an anti-plane elastic solid. The governing equation is chosen with Griffith's theory in mind. The following equation (3.1) that defines the total energy of an elastic body with a smeared crack was selected as the governing equation.

$$\mathrm{E}\,(u,v) = \int_{\Omega} v^2 W(\nabla u)\, d\Omega + \int_{\Omega} \left[\frac{(1-v)^2}{4\kappa} + \kappa |\nabla v|^2 \right] d\Omega \tag{3.1}$$

The energy functional equation above maps the functions *v*, representing the crack phase-field parameter, and *u*, which is mechanical displacement, defined over the region Ω to the total energy of the elastic body. The two integrals define the elastic energy stored in the cracked body, and the second integral represents the energy required for a crack to propagate, as stated in Griffith's theory. The crack surface density function was taken in its original proposed form, with κ as its phase-field regularization parameter. The first term is a penalization term that discourages values of *v* away from 1. The second term is a regularization term that penalizes large gradients of *v*. As the problem is an anti-plane problem, the elastic potential becomes:

$$W(\nabla \mathrm{u}) = \int_{\Omega} \frac{\mu}{2} (\nabla u_z)^2 \, d\Omega \tag{3.2}$$

3.1.2 MATLAB Coding

We can obtain two governing elliptic PDEs to solve the above defined governing equations. The PDEs are obtained by minimizing the total energy of the system with respect to *u* and *v*. To solve the given equations, we take use of MATLAB's PDE Toolbox. It is a toolbox for MATLAB software that provides functions for solving partial differential equations using numerical methods. The toolbox supports the solution of linear and non-linear PDEs, including time-dependent and stationary problems. It supports finite element, finite difference, and other numerical methods for solving PDEs, and includes functions for performing tasks such as meshing, discretization, and post processing of solutions. For convenience, the elastic potential and other equations are rewritten into an expected and easily readable form by the PDE toolbox.

$$au - c \cdot \nabla^2 u = f \tag{3.3}$$

The parameters *a*, *c*, and *f* are to be properly defined and fed into the toolbox accordingly to the two PDEs. The code starts with defining important variables, it defines the total steps, and the time interval between steps. For the anti-plane elasticity parameters, the shear modulus of the material is defined as 'μ'. The Initializing crack phase-field parameter is defined as $v_t = 1$. For our phase-field problem, non-crack regions are signified with *v* value as 1 and *v = 0* signifies crack region. κ is the regularization parameter for the phase-field gradient of *v*. The parameters a_1 and f_1 for the elastic problem PDE are given a value of zero. The parameters c_2 and f_2 for the phase-field crack problem PDE are defined as:

$$c_2 = 2.\kappa \tag{3.4}$$

$$f_2 = \frac{1}{2.\kappa} \tag{3.5}$$

After defining all variables and initial parameters, PDE models are made with a single dependent variable for the anti-plane displacement variable u and Phase-field parameter v each, as pdem1 and pdem2 respectively.

The geometry of the anti-plane elastic solid is defined with the DECSG function using subtraction to cut notches into a rectangular specimen. The width, height, notch position, notch length, and notch half-width are defined with the gdm1 matrix that is fed to the DECSG function along with the set formula that creates a DECSG geometry out of them. After converting it into a geometry model it can be appended to the PDE models pdem1 and pdem2. The mesh is created as a linear triangular mesh on the geometry setting an appropriate maximum element size.

The PDE models are then solved within a loop to minimize energy with respect to the values of *u* and *v*. For the boundary conditions, the top and bottom edges are subjected to a displacement on the top and bottom edges with a displacement u that increases with each step in steady increments of DeltaT. For initialization, $v_t = 1$, and *ElasticEnergy = 0*. The c_1 value for the elastic problem is assigned as a function of the v_t value.

$$c_1 = {v_t}^2 . \mu \tag{3.6}$$

The elastic problem PDE is solved using the elliptic solver. The "assempde" function is used to assemble the PDE problem with data pdem1, c_1, a_1, and f_1 and solves for u, where u is stored in a matrix with each column corresponding to a time step. The function "pdegrad" is then used to calculate the gradient of u in the x and y directions, represented by dudx and dudy respectively. The variable "area" is then calculated using the "pdetrg" function which computes the area of the triangles formed by the mesh points in the region Ω. Next, the elastic energy is calculated as:

$$ElasticEnergy = \frac{\mu}{2}\left(\frac{du^2}{dx} + \frac{du^2}{dy}\right) \tag{3.7}$$

Finally, the function "pdeprtni" is used to compute the integral of the elastic energy over the region Ω. The result is stored in the variable u.

For the irreversibility condition, the code loops over all elements in the mesh represented by the triangles t and checks the value of v_t at each element. If v_t is less than 0.005, then the corresponding value of ElasticEnergy is set to the maximum value of ElasticEnergy for that element, represented by MaxElasticEnergy. This irreversibility condition ensures that the energy in the system does not decrease during the time-stepping process.

The phase-field crack problem parameter a_2 is assigned a proper value in the loop with the formula:

$$a_2 = 2\left(ElasticEnergy + \frac{1}{4 . k}\right) \tag{3.8}$$

The Phase-field crack problem is then solved using elliptic solver again. The "assempde" function is used again to assemble the PDE problem with data pdem2, c_2, a_2, and f_2 and it solves for v, where v is stored in a matrix with each column corresponding to a time step. The function "pdeintrp" is then used to interpolate the nodal values of the solution v on the elements of the mesh, represented by the triangles t. The result is stored in the variable v_t.

The loop repeats with this value of v_t for the set total steps, chosen so that the crack propagation pattern can properly be developed. The PDE models after the total steps

are plotted using the pdeplot function for u and v as contour plots. This gives us a proper diagram for crack propagation that can be used for analysis.

3.1.3 MATLAB Simulation

After coding is done in MATLAB, a sample problem is selected that can be used for crack simulation for a notched specimen. Multiple such experiments can be simulated to test the feasibility of the code and problems can be run on different parameters to find any limitations that the code possesses. The simulation was done with a square specimen with two notches in each side with variable lengths and widths over different positions on the sides of the specimen so that crack propagation can be observed on different configurations of notches.

A second problem was taken as a benchmark test from multiple papers, with a single 2D notched square plate with geometry as shown in *Figure 3.2* subjected to tension given by displacement *u*.

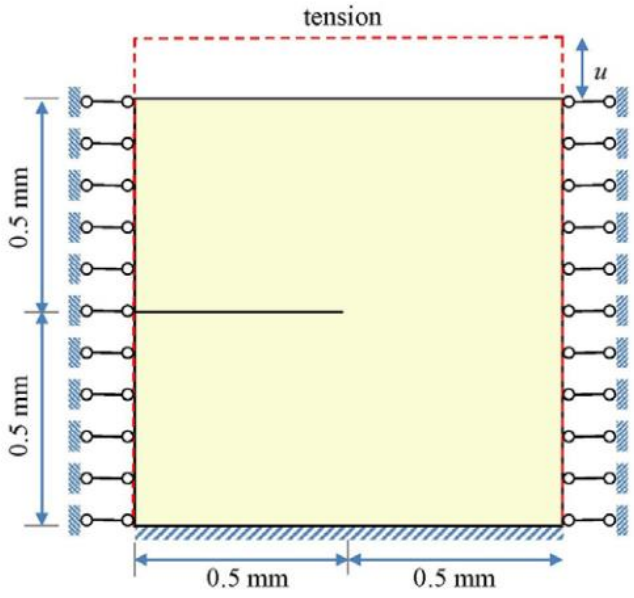

Figure 3.2: Geometry and boundary conditions for sample benchmark test [7]

The simulation was done in 30 total steps with a time increment of 0.1 seconds. Shear modulus was taken as 10 GPa, and the value of the phase-field regularization parameter was taken according to the length scale of the specimen for different problems.

3.1.3.1 Flowchart for MATLAB Code

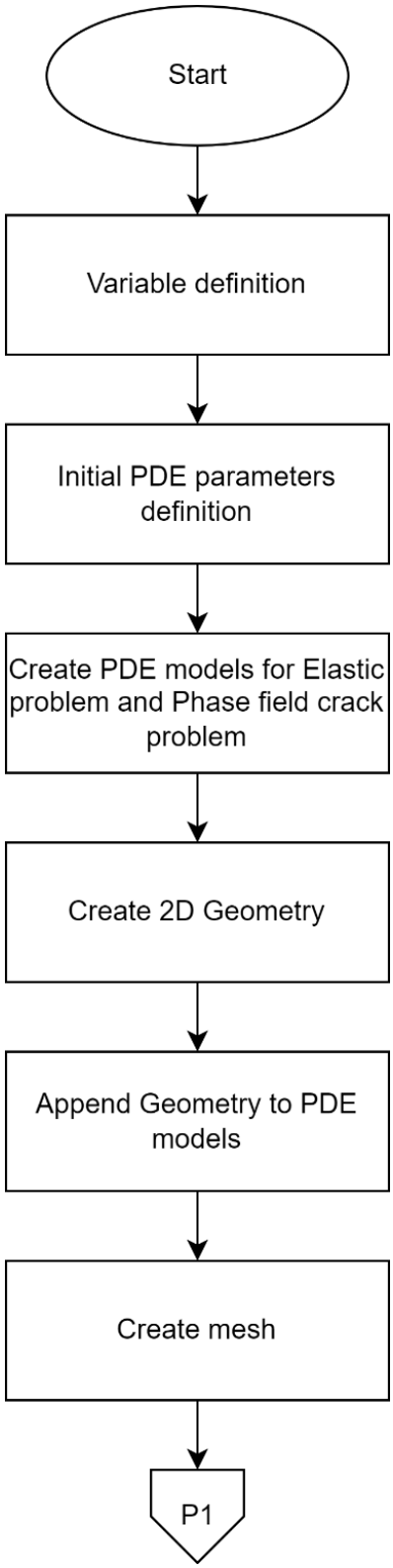

Figure 3.3: Flowchart for MATLAB code (part 1)

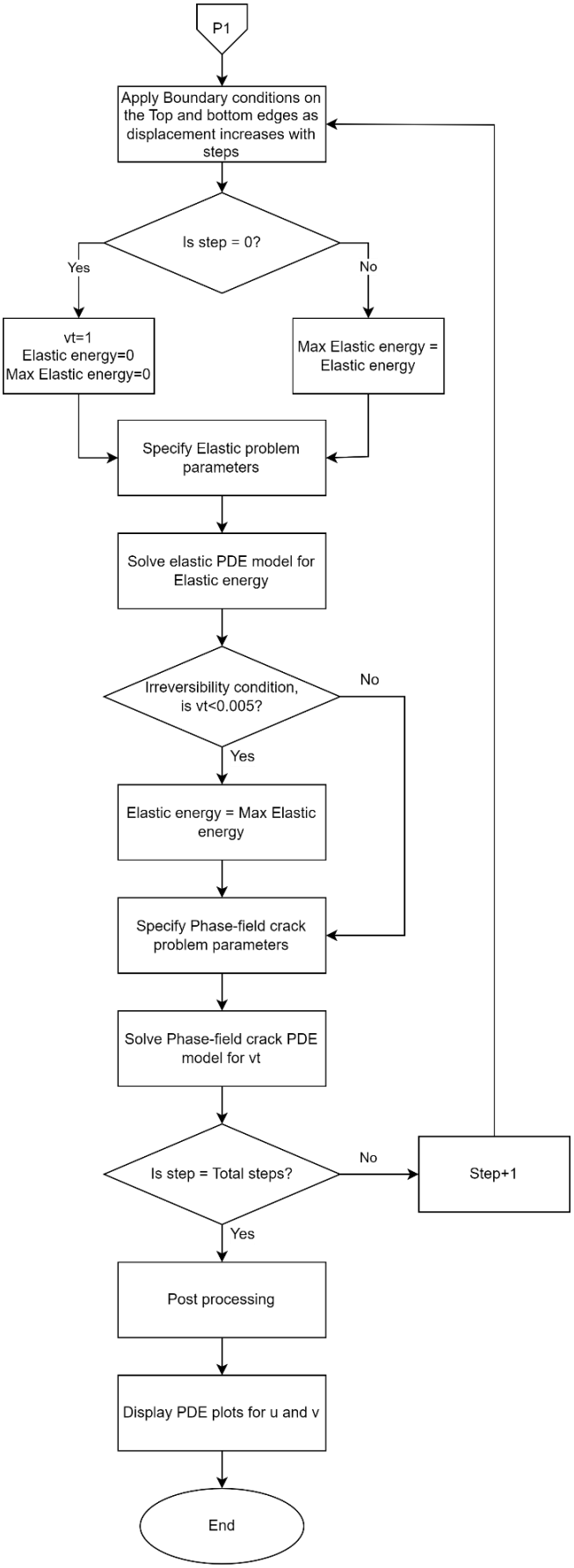

Figure 3.4: Flowchart for MATLAB code (part 2)

3.1.4 Analysis of Results

Simulations were done firstly testing the benchmark test and then onto using the two notched problems varying specimen geometry by changing the notch geometry and location along the sides of the specimen to observe the crack propagation results. A crack propagation pattern would be observed for each configuration of geometry. The results would be analyzed with their phase-field plots and displacement plots to compare the code's performance.

3.1.5 Experimental Validation

For experimental validation, a suitable specimen was chosen first taking into account the required material properties and availability. A 2 mm thin plate of mild steel was taken and cut into four pieces of dimensions 130x63 mm for one and 154x70 mm for the other three. Each test specimen was added with around 50 mm long clamping metal with width 5 mm each welded together on each side of the plate to account for the grips spacing in the UTM. The notches for specimen having dimension 130x60 mm were kept at a distance of 27% from nearest edge on each side on opposite directions. *Figure 3.5* gives us geometry model for test piece 1, and *Figure 3.6* shows the fabricated test piece for UTM testing.

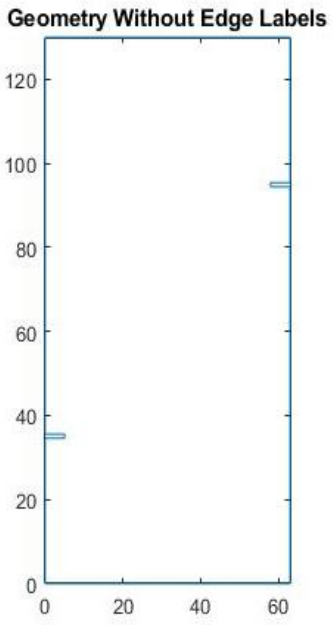

Figure 3.5: Geometry for test specimen 1

Figure 3.6: Test specimen 1

The second and third specimens of dimensions 154x70 mm were added with notches at 40% from nearest edge on each side on opposite directions. *Figure 3.7* gives the geometry model for test pieces 2 and 3 and the finished machined test specimen 2 is shown in *Figure 3.8.*

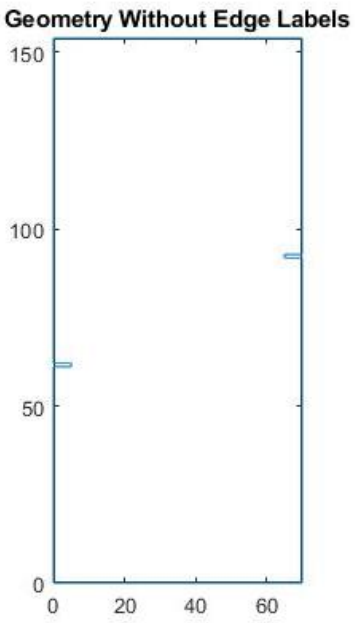

Figure 3.7: Geometry for test specimen 2 and 3

Figure 3.8: Test piece 2

The final piece of dimensions 154x70 mm was added with no notches to account for the energy loss due to welding.

Each of the specimen were fitted into the UTM for testing and put under tension load until failure noting down the force and displacement values in the computer.

CHAPTER FOUR: RESULTS AND DISCUSSION

4.1 Mesh Independence and Convergence Test

A mesh convergence test was performed on the test piece keeping the value of the phase-field regularization parameter constant at 0.6 mm on test piece 2. The mesh maximum size was varied from 0.3 mm to 1.2 mm with differences of 0.05 mm in each step, plotting for values of peak load. The final plot for number of elements vs peak load is as shown in *Figure 4.1*. Form this a suitable mesh element number can be selected as 265,678 elements, corresponding to a maximum mesh element length of 0.3 mm.

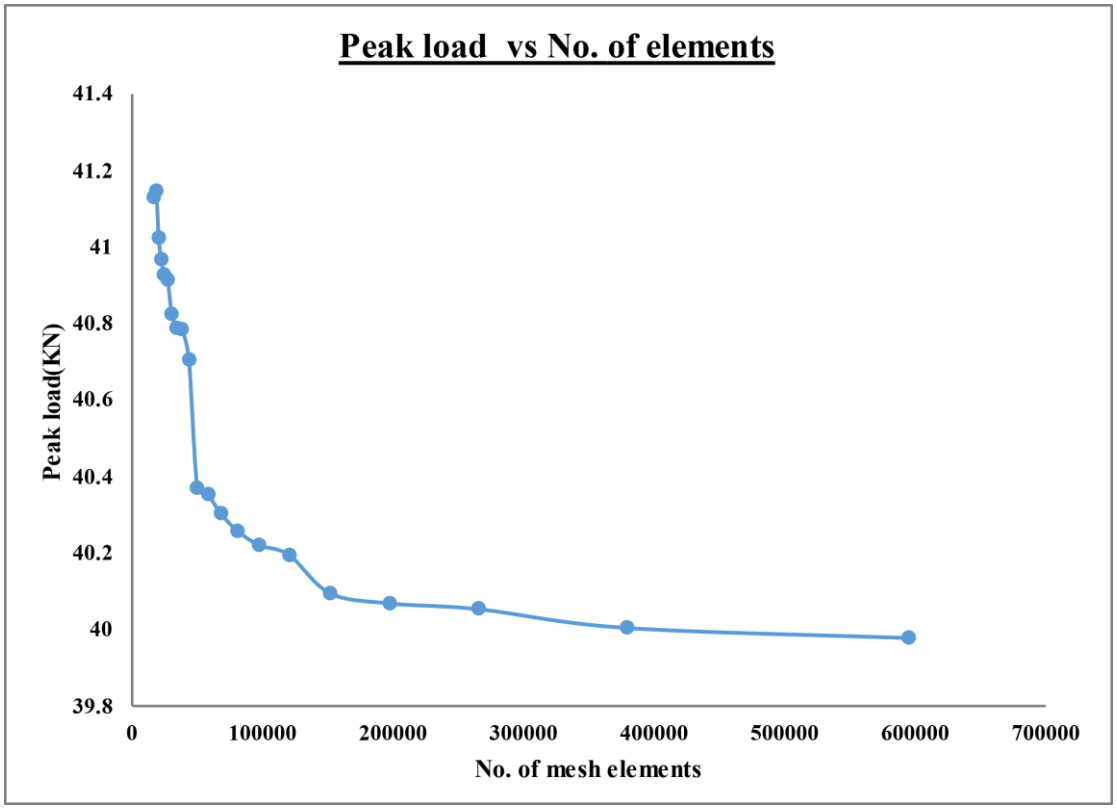

Figure 4.1: Mesh independence test

4.2 Variation of Shear Modulus

The code was run first with a test problem of rectangle anti-plane solid having two notches on each side given a set displacement over each time interval. A 2x2 mm anti-plane solid with shear modulus 10 GPa was taken with triangular notches of length 0.2 mm and width 0.1 mm. The notches were placed on 20% of height on the left side and 80% of height on the right side. The geometry of test sample can be seen in the *Figure 4.2*. The code was run with a displacement of 0.1 mm per step for 30 steps on the top edge and the bottom edge kept fixed and the crack patterns were observed with the phase-field parameter contour plot in *Figure 4.4* and the sharp crack interface can be approximated using the displacement distribution plot in *Figure 4.5.*

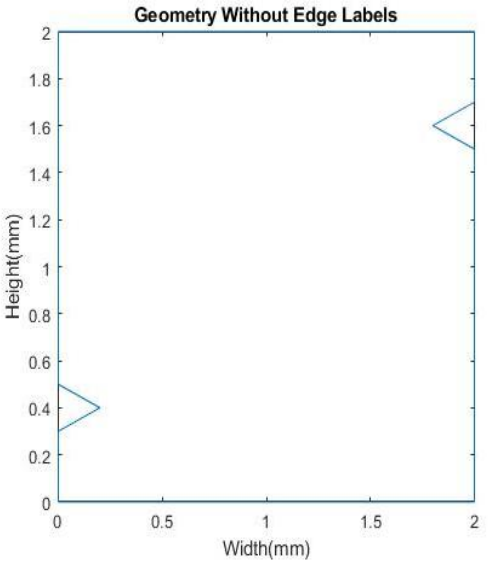

Figure 4.2: Geometry for sample problem 1

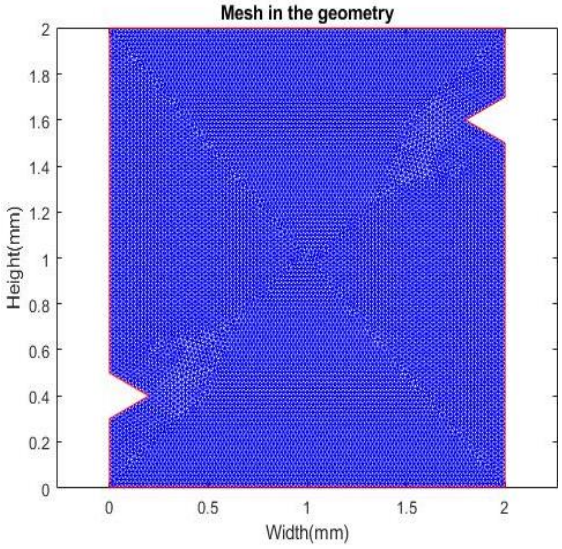

Figure 4.3: Mesh for sample problem 1

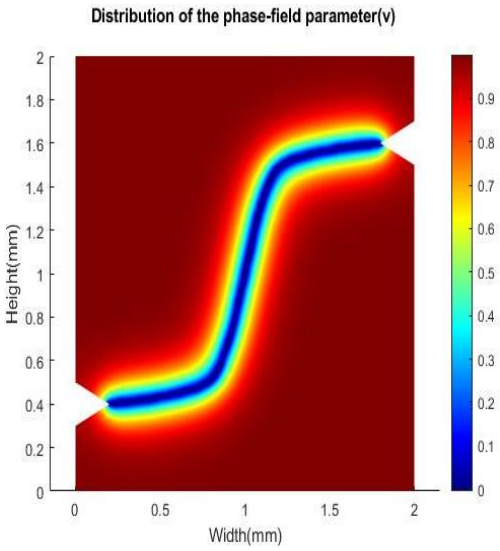

Figure 4.4: Phase-field parameter distribution in sample problem 1

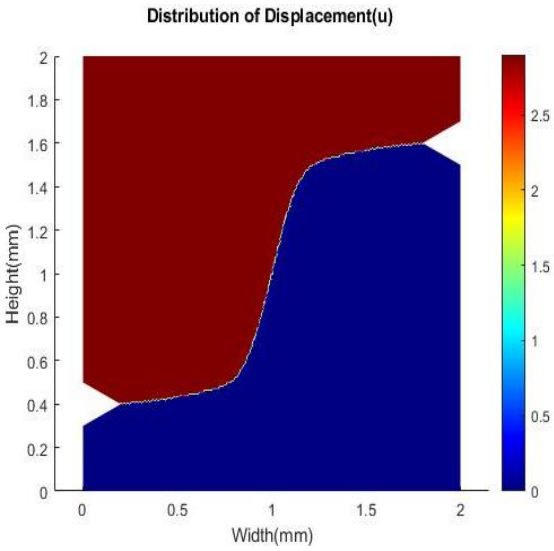

Figure 4.5: Displacement distribution in sample problem 1

The code was run again for two-notched problem with same geometry changing shear modulus to 77 GPa, with the same geometry as shown in *Figure 4.6*. The resultant phase-field contour plot and displacement contour plot can be seen in *Figure 4.7* and *Figure 4.8* respectively.

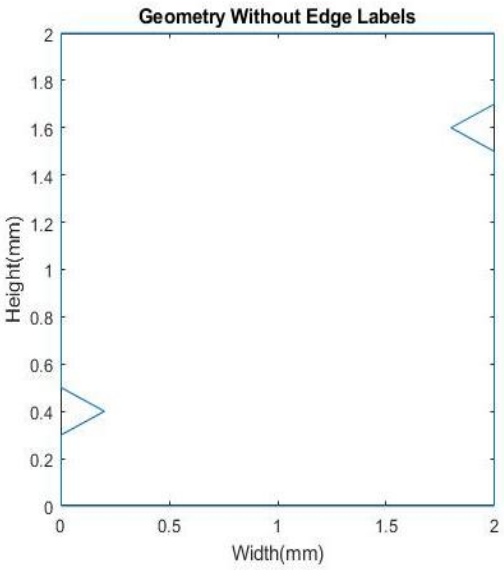

Figure 4.6: Geometry for sample problem 2

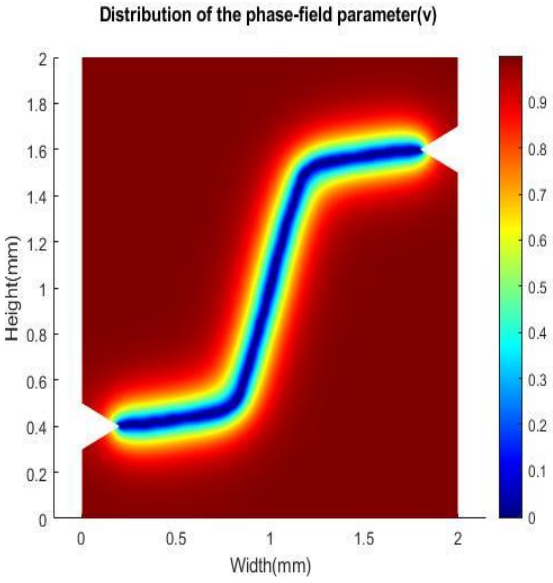

Figure 4.7: Phase-field parameter distribution in sample problem 2

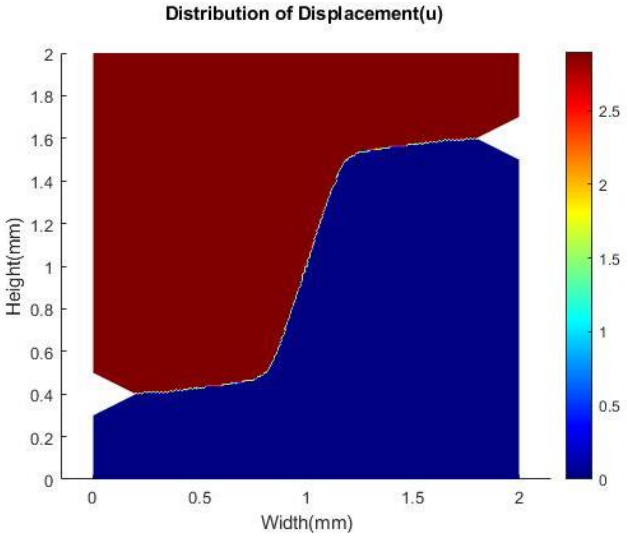

Figure 4.8: Phase-field parameter distribution in sample problem 2

In conclusion, change in shear modulus does not bring any change in the final crack propagation pattern of the solid plate. However, there is a difference in crack propagation between the two materials of different shear modulus when steps for both materials is kept at a third of their total steps.

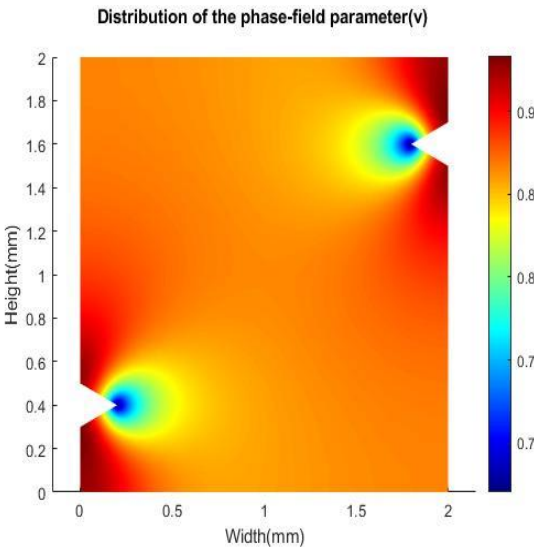

Figure 4.9: Phase-field parameter distribution in sample problem 1 at step=10

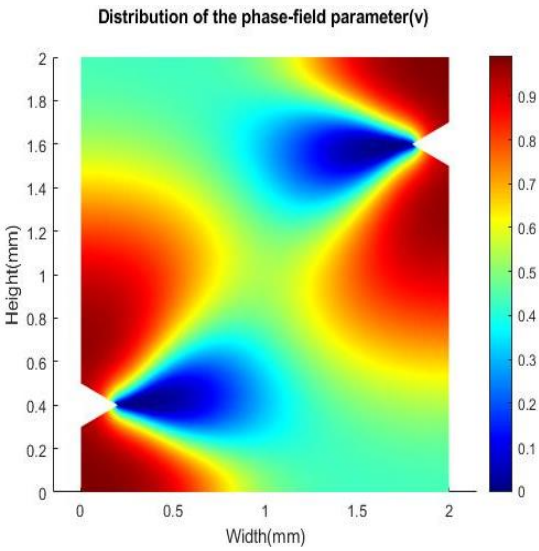

Figure 4.10: Phase-field parameter distribution in sample problem 2 at step=10

From the comparison of two contour plots *Figure 4.9* and *Figure 4.10* , the crack formation for sample problem 1 is already apparent while for sample problem 2, crack formation is still in progress.

4.3 Benchmark Test

For the benchmark test, a single thin notch was placed on the same 1x1 mm square specimen with a thin notch on the halfway location of the left side going inwards 0.5 mm as shown in *Figure 4.11*. A regular displacement is kept on the top edge as above examples and the bottom is kept fixed. The shear modulus was kept as 210 GPA, and with a mesh size of 7.5×10^{-3} mm.

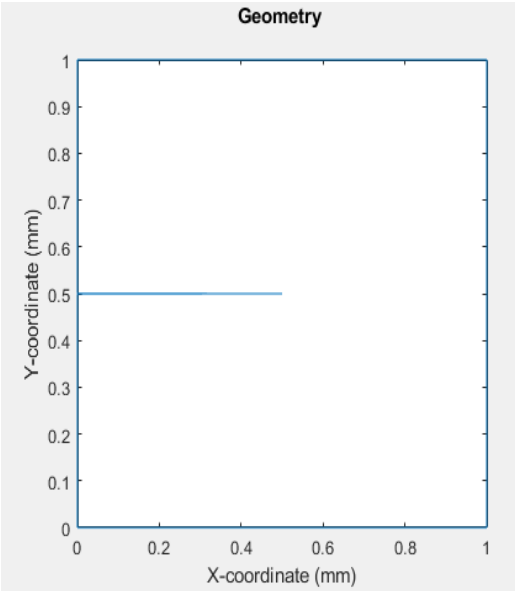

Figure 4.11: Geometry for sample problem 3

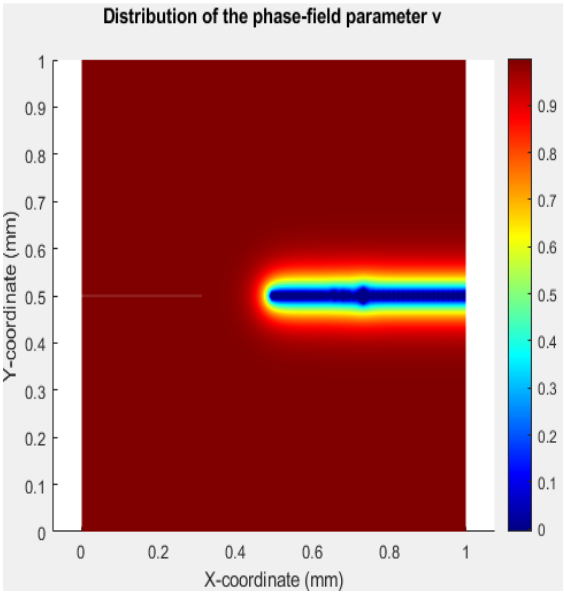

Figure 4.12: Phase-field parameter distribution in sample problem 3

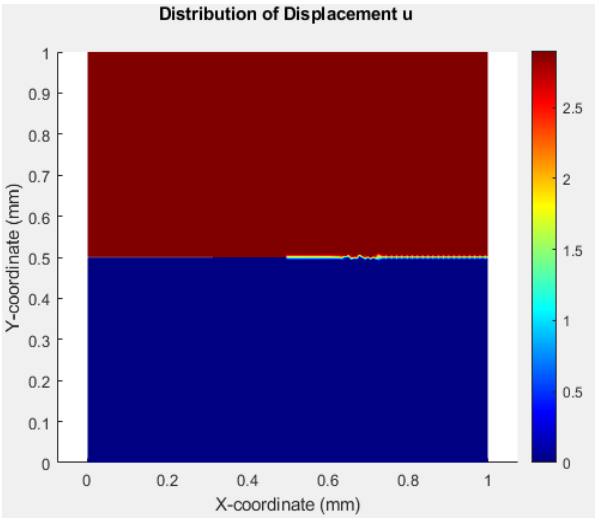

Figure 4.13: Displacement distribution in sample problem 3

The crack patterns thus obtained as shown in *Figure 4.12* and *Figure 4.13* were within expectation and benchmark test was concluded.

4.4 Branching

Our code is also capable of handling the branching of cracks. For testing the branching of cracks a simulation was done by creating a geometry as shown in *Figure 4.14* , with three notches, one notch on one side and the other notches at equal distances to the first notch on the other side. After the simulation the crack propagation was seen to be smooth, propagating from one notch and branching to the two notches on other sides as shown in the *Figure 4.15*.

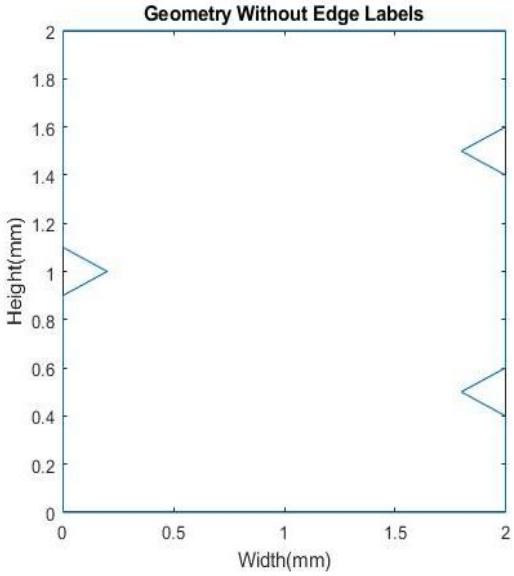

Figure 4.14: Three-notched geometry

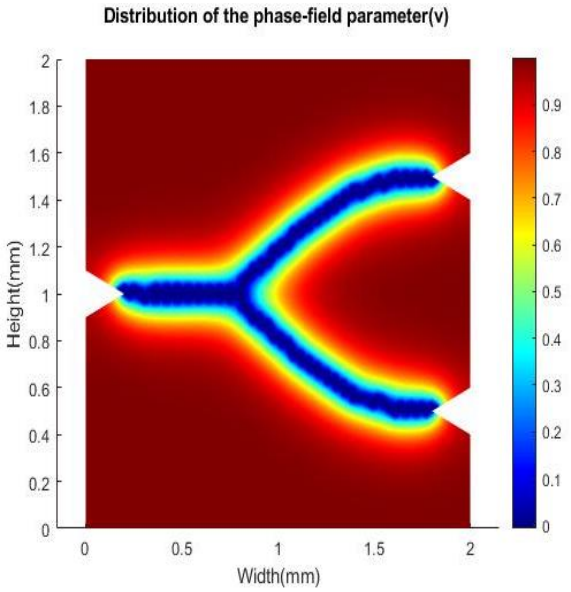

Figure 4.15: Phase-field parameter distribution in three-notched geometry

4.5 Circular Void

To test the robustness of the code we induced the crack in a more complex geometry. We added a circular void in the middle of a square shaped geometry and simulated it by fixing the circumference of the circular void and applying tensile load at top edge of the square as shown in *Figure 4.16*. The MATLAB code gave phase-field plot as shown in *Figure 4.17*. The code was able to simulate the crack propagation in the same way as [7].

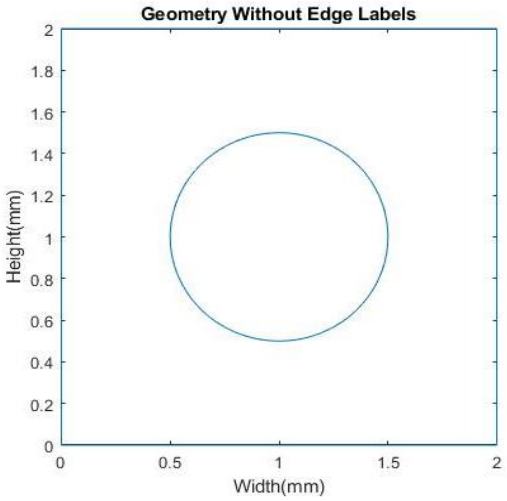

Figure 4.16: Geometry with circular void

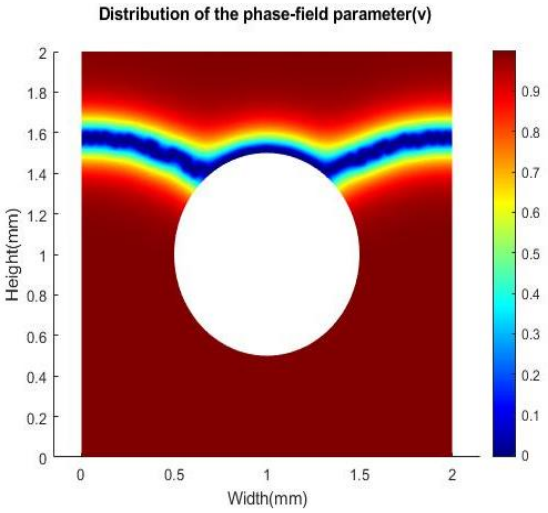

Figure 4.17: Phase-field parameter distribution in geometry with circular void

4.6 Experimental Validation

4.6.1 Test Specimen 1

The results from MATLAB and UTM testing for test specimen 1 can be seen in *Figure 4.18* and *Figure 4.19* respectively.

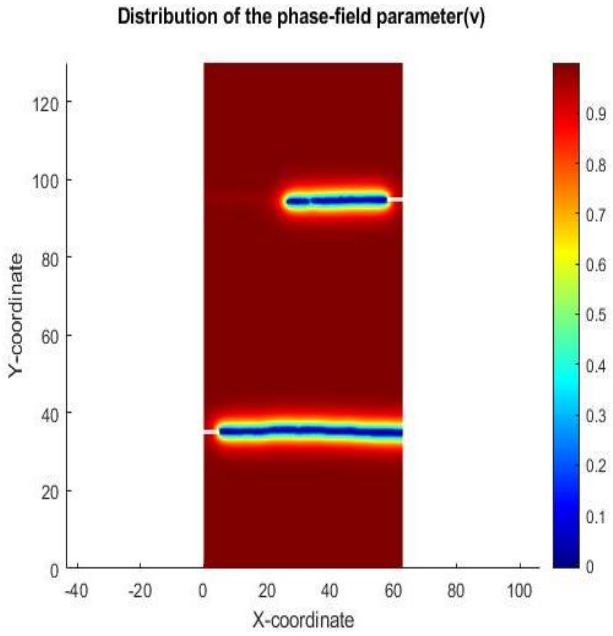

Figure 4.18: Phase-field parameter distribution for test specimen 1

Figure 4.19: Test specimen 1 after UTM testing

The first specimen of 130x63 mm dimension was seen to have notches too far apart that resulted in crack propagating straight from notch to the other side. The bottom notch was seen to have been the first to cause failure. The pattern of crack propagation obtained from UTM testing in test specimen 1 yielded similar results to that of MATLAB.

4.6.2 Test Specimens 2 and 3

The non-notched specimen was tested first with the UTM to find maximum possible peak load allowable due to welding effects, which turned out to be 56 KN for test specimen 2 and 3. The result from MATLAB and UTM testing for test specimen 3 can be seen in *Figure 4.20* and *Figure 4.21* respectively.

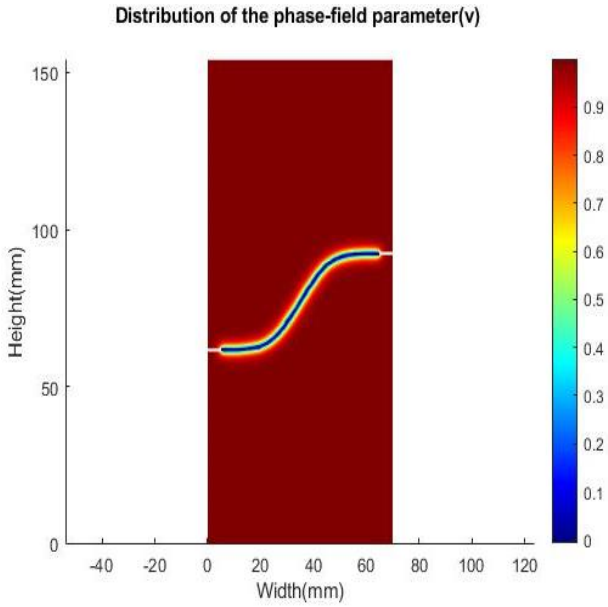

Figure 4.20: Phase-field parameter distribution for test specimens 2 and 3

Figure 4.21: Test specimen 3 after UTM testing

The simulation results for test specimens 2 and 3 displayed an S-shaped crack pattern as shown in *Figure 4.20* that is formed due to joining of crack tip from each notch. For test specimen 3, the crack pattern from UTM tensile testing was observed to be similar to that observed in the simulation as shown in *Figure 4.21*, where the crack from two notches met together to form one crack pattern.

For the test specimen 2, the crack pattern from UTM tensile testing as shown in *Figure 4.22* resulted in a different pattern of crack propagation than MATLAB simulation, which could be accounted for by the improper alignment of test piece.

Figure 4.22: Test specimen 2 after UTM testing

4.6.3 Comparison Between MATLAB and UTM Data

Between the load vs displacement graphs plotted for UTM data and the simulation data, the peak load for Simulation was 58.245 KN and from UTM, it was observed to be 58 KN for test specimen 1. For test specimen 3, the peak load for simulation was 40.054 KN and from UTM, it was 43.65 KN. The threshold test that was done to exclude the possibility of welding causing any cracks in the specimen yielded a peak load value of 56 KN which is below the 43.65 KN peak load for test specimen 3. The graphs trace a similar pattern of progression for simulated and experimented data, where load steadily increases until a maximum value then plummets when failure occurs due to crack formation and load decreases. The experimental results had graph with irregular increase in maximum load due to it not being a perfectly elastic solid which is assumed in the simulation.

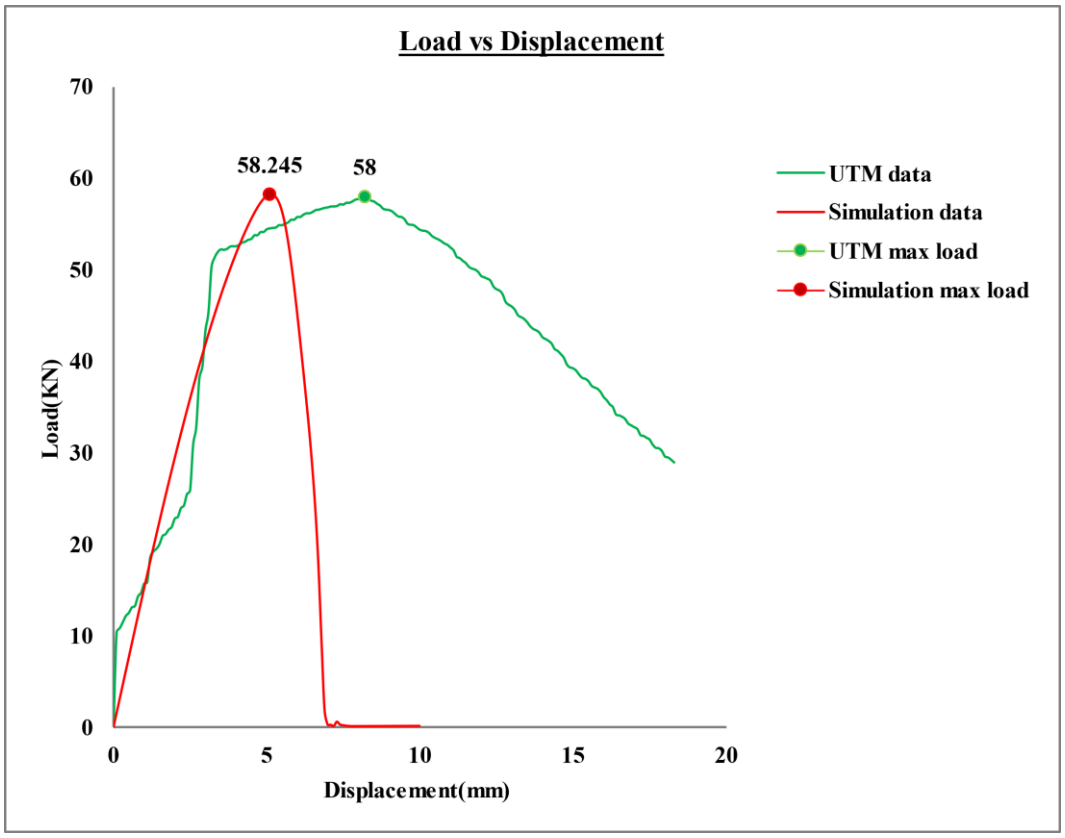

Figure 4.23: Load vs Displacement graph for test specimen 1

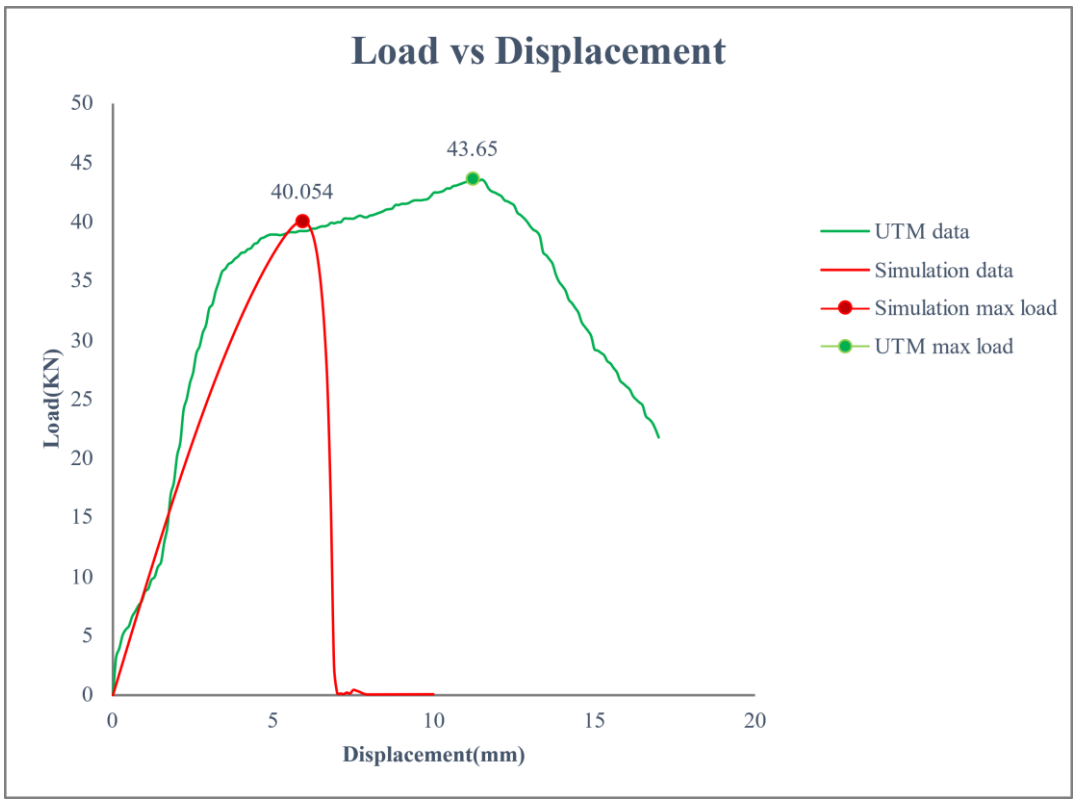

Figure 4.24: Load vs Displacement graph for test specimen 2

The crack patterns obtained from simulation were thus effective in predicting the crack pattern that had been experimentally observed. However, there were significant differences to the plot data due to property of the material, alignment of specimen in UTM and human errors.

4.6.4 Effect of Welding

Initially, a mild steel specimen was taken as a test piece to analyze the crack propagation. The length, width, and thickness of the specimen was 150 mm, 70 mm and 2 mm respectively. The specimen was welded with around 40 mm long clamping metal with thickness 5 mm on each side of the plate at the end which is to be clamped in the UTM such that the effective length is 70 mm. Two notches of length 5 mm and width 1 mm were created 30% in length from both the edges where they were clamped in opposite directions. The geometry in MATLAB is as it is in *Figure 4.25*. In the simulation, the crack propagated from one notch to the other, shown in *Figure 4.27*, but during experiment, the test piece developed crack as shown in *Figure 4.26*. The crack propagated from one notch to the welding point.

To analyze this problem, we created another notch at the same welding point. We found from the phase-field plot in *Figure 4.28* that crack propagated from one notch to a notch that had been formed at the welding point due to high heat. Thus, we concluded that due to welding the material property is changed and needs less energy to break and during elongation welding point is the lower energy point.

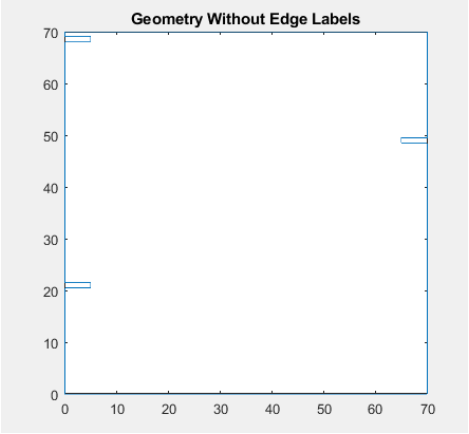

Figure 4.25: Geometry for initial test specimen

Figure 4.26: Initial test specimen after UTM testing

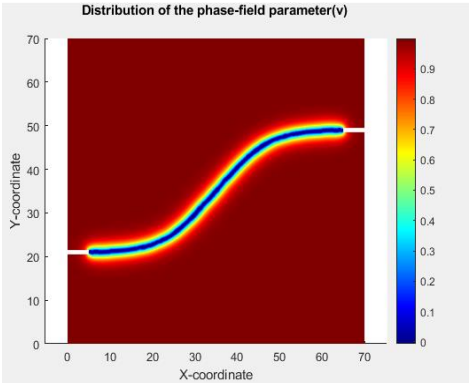

Figure 4.27: Phase-field parameter distribution in initial test piece without welding defect

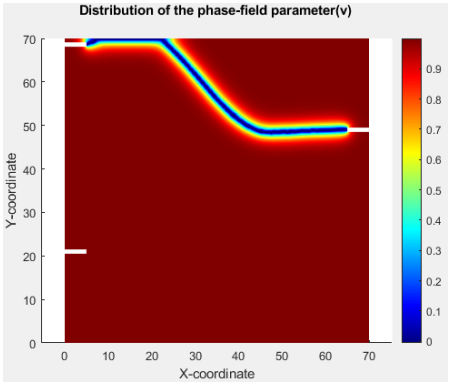

Figure 4.28: Phase-field parameter distribution in initial test piece with welding defect

4.6.5 Transition from Single to Separate Cracks

To figure out the transition distance from when the two cracks join to form an S shape and when they go straight through without joining up, simulation is run for the two specimens, as shown in *Figure 4.29* and *Figure 4.30* with distance between notches varying with percentage of total length. After MATLAB simulation, it is found that for both cases of width and length, the transition occurs when the distance between two notches is somewhere between 30% and 35%.

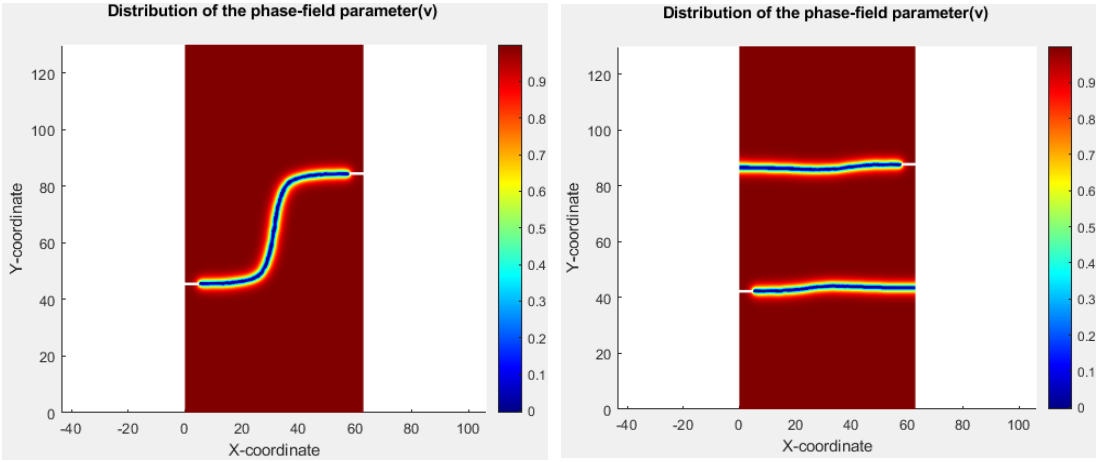

(a) *(b)*

Figure 4.29: Phase-field parameter distribution in test specimen 1 with notches at a difference
(a) 30% and (b) 35% specimen length from each other respectively

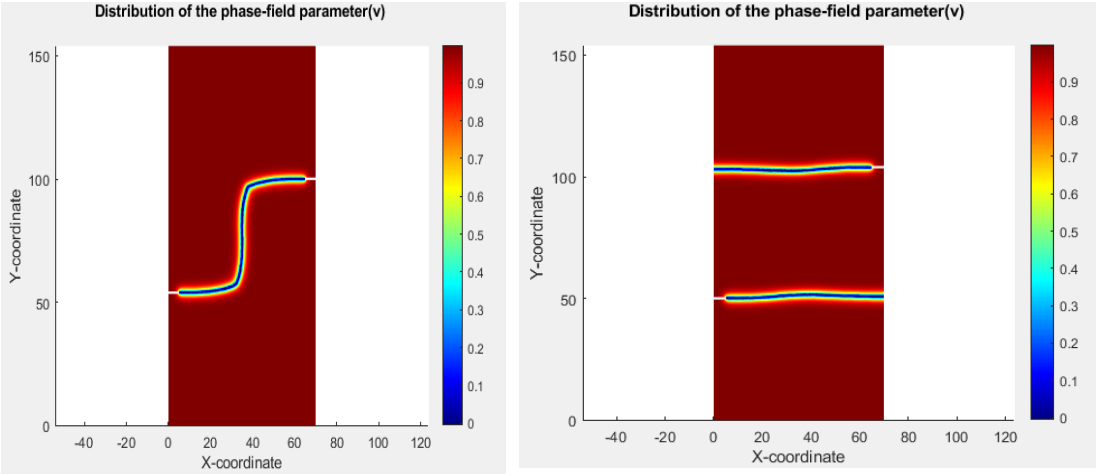

(a) *(b)*

Figure 4.30: Phase-field parameter distribution in test specimen 2 with notches at a difference
(a) 30% and (b) 35% specimen length from each other respectively

When the gap between two notches is small, the stress concentration due to one notch overlaps the stress concentration due to another notch. Due to this condition, there is a higher overall stress concentration at the crack tip and the propagation of the crack is accelerated. Ultimately, it results in failure of the material.

When the gap between two notches is large, there is no overlap in stress concentration. This reduces the stress concentration at the crack's tip and the crack propagation process is slowed down.

4.7 Limitations

The limitations of our project are:

i. The accuracy of code is defined for brittle materials only.
ii. The code is restricted to second order differential equation.
iii. The working of code is restricted to 2D geometries.

4.8 Problems Faced

The major problem we faced during the project is finding a suitable governing equation and implementing it for the development of code. Very few researches have been done in the field of crack propagation using phase-field model. Due to this reason, it was difficult to find a relatable governing equation. Selection and availability of material for experimental validation was also a major challenge. The simulations were done assuming no brittle fracture on a perfectly elastic body. Though the code was developed for brittle fracture due to the issues of availability and machinability the governing equations were done imagining a 2D solid with anti-plane loading so significant differences were obtained from the experimental results.

4.9 Work Schedule

Table 4.1: Work Schedule

S.N.	WORK	TIME FRAME
1	Literature Study	9 months
2	Proposal Writing	2 weeks
3	Studying Governing Equations and Related Parameters	2 weeks
4	Development of Code	10 weeks
5	Analysis of Result	2 weeks
6	Improvement of Code	8 weeks
7	Mid Term Report Preparation	4 weeks
8	Experimental Setup	2 weeks
9	Validation of Code	4 weeks
10	Final Report Preparation	4 weeks

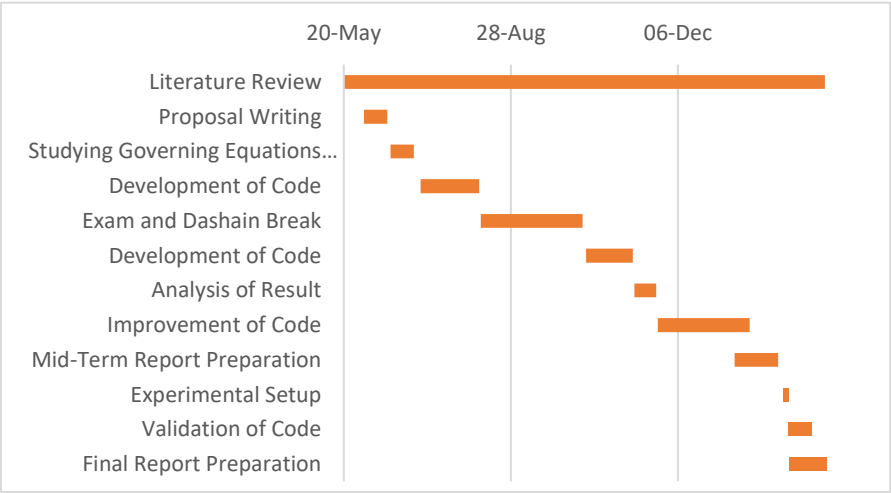

Figure 4.31: Gantt chart

CHAPTER FIVE: CONCLUSION AND FUTURE ENHANCEMENT

5.1 Conclusion

Generally, crack in the material constitute of a discontinuous interface between the crack and the matrix. Usual methods for computation of crack propagation would involve arduous use of re-meshing and tracking the crack's tip to simulate propagation. The phase-field method bases its calculation on the minimum energy principle, which is used alongside a continuous phase-field variable that separates non-crack and crack with values of one and zero respectively and assumes their interface to be a continuous gradient which smoothly changes value from crack to non-crack over a thin phase-field length. The phase-field problem used in this project has a governing equation that solves for minimum elastic energy using two functions *v*, the phase-field parameter and *u*, the mechanical displacement over an area domain for an anti-plane elastic solid. The equations were solved using PDE models that were computed using FEM methods in MATLAB using its PDE Toolbox. Various problems were proposed to show the effects produced by varying shear modulus and crack location and geometry. Experimental verification was done with the simulated results using UTM to compare the code with real life application, giving us the value for peak loads during fracture to be $58\ KN$ for test specimen 1 and $43.65\ KN$ for test specimen 2. The analysis of result demonstrates the efficiency of phase-field method as an efficient tool for the numerical simulation of crack propagation in an anti-plane elastic solid problem.

5.2 Scope for Future Enhancements

The project can be further enhanced in the future in the following ways:

i. The code can be improved to work on 3D geometries.

ii. The governing equation and code can be further developed for ductile materials.

iii. The propagation of crack can be done using other computational methods like XFEM and the accuracy of these techniques can be compared.

iv. Study of cracks with respect to change in parameters like critical energy release rate and residual stress in ductile fracture.

REFERENCES

[1] T. Rabczuk, "Computational Methods for Fracture in Brittle and Quasi-Brittle Solids: State-of-the-Art Review and Future Perspectives," *ISRN Applied Mathematics,* vol. 2013, pp. 1-38, 2013.

[2] M. J. Borden, C. V. Verhoosel, M. A. Scott, T. J. R. Hughes and C. M. Landis, "A phase-field description of dynamic brittle fracture," *Computer Methods in Applied Mechanics and Engineering,* Vols. 217-220, p. 77–95, April 2012.

[3] A. A. Griffith, "VI. The phenomena of rupture and flow in solids," *Philosophical Transactions of the Royal Society of London. Series A, Containing Papers of a Mathematical or Physical Character,* vol. 221, pp. 163-198, January 1921.

[4] G. R. Irwin, "Linear fracture mechanics, fracture transition, and fracture control," *Engineering Fracture Mechanics,* vol. 1, pp. 241-257, August 1968.

[5] G. A. Francfort and J.-J. Marigo, "Revisiting brittle fracture as an energy minimization problem," *Journal of the Mechanics and Physics of Solids,* vol. 46, pp. 1319-1342, August 1998.

[6] B. Bourdin, G. A. Francfort and J.-J. Marigo, "Numerical experiments in revisited brittle fracture," *Journal of the Mechanics and Physics of Solids,* vol. 48, pp. 797-826, April 2000.

[7] X. Zhuang, S. Zhou, G. D. Huynh, P. Areias and T. Rabczuk, "Phase-field modeling and computer implementation: A review," *Engineering Fracture Mechanics,* vol. 262, p. 108234, March 2022.

[8] C. Miehe, M. Hofacker and F. Welschinger, "A phase-field model for rate-independent crack propagation: Robust algorithmic implementation based on operator splits," *Computer Methods in Applied Mechanics and Engineering,* vol. 199, p. 2765–2778, November 2010.

[9] C. Kuhn, Numerical and Analytical Investigation of a Phase-field Model for Fracture, 2013.

[10] J. M. Sargado, E. Keilegavlen, I. Berre and J. M. Nordbotten, "High-accuracy phase-field models for brittle fracture based on a new family of degradation functions," *Journal of the Mechanics and Physics of Solids,* vol. 111, pp. 458-489, February 2018.

[11] L. Ambrosio and V. M. Tortorelli, "Approximation of functional depending on jumps by elliptic functional via t-convergence," *Communications on Pure and Applied Mathematics,* vol. 43, pp. 999-1036, December 1990.

[12] H. Amor, J.-J. Marigo and C. Maurini, "Regularized formulation of the variational brittle fracture with unilateral contact: Numerical experiments," *Journal of the Mechanics and Physics of Solids,* vol. 57, pp. 1209-1229, August 2009.

[13] S. Ramanathan, D. Ertaş and D. S. Fisher, "Quasistatic Crack Propagation in Heterogeneous Media," *Physical Review Letters,* vol. 79, pp. 873-876, August 1997.

[14] R. Spatschek, E. Brener and A. Karma, "Phase-field modeling of crack propagation," *Philosophical Magazine,* vol. 91, pp. 75-95, January 2011.

[15] X. Lu, C. Li, Y. Tie, Y. Hou and C. Zhang, "Crack propagation simulation in brittle elastic materials by a phase-field method," *Theoretical and Applied Mechanics Letters,* vol. 9, p. 339–352, November 2019.

[16] C. Schreiber, R. Müller and C. Kuhn, "Phase-field simulation of fatigue crack propagation under complex load situations," *Archive of Applied Mechanics,* vol. 91, pp. 563-577, November 2020.

[17] H. Li, W. Wang, Y. Cao and S. Liu, "Phase-Field Modeling Fracture in Anisotropic Materials," *Advances in Civil Engineering,* vol. 2021, pp. 1-13, July 2021.

[18] X. Zhang, C. Vignes, S. W. Sloan and D. Sheng, "Numerical evaluation of the phase-field model for brittle fracture with emphasis on the length scale," *Computational Mechanics,* vol. 59, pp. 737-752, January 2017.

[19] F. Zhang, W. Huang, X. Li and S. Zhang, "Moving mesh finite element simulation for phase-field modeling of brittle fracture and convergence of Newton's iteration," *Journal of Computational Physics,* vol. 356, pp. 127-149, March 2018.

[20] A. T. Zehnder, "Griffith Theory of Fracture," *Encyclopedia of Tribology,* pp. 1570-1573, 2013.

[21] J.-Y. Wu, V. P. Nguyen, C. T. Nguyen, D. Sutula, S. Sinaie and S. P. A. Bordas, "Phase-field modeling of fracture," *Advances in Applied Mechanics,* pp. 1-183, 2020.

[22] J.-Y. Wu, "A unified phase-field theory for the mechanics of damage and quasi-brittle failure," *Journal of the Mechanics and Physics of Solids,* vol. 103, p. 72–99, June 2017.

[23] K. Weinberg, T. Dally, S. Schuß, M. Werner and C. Bilgen, "Modeling and numerical simulation of crack growth and damage with a phase-field approach," *GAMM-Mitteilungen,* vol. 39, pp. 55-77, May 2016.

[24] K. Weinberg and C. Hesch, "A high-order finite deformation phase-field approach to fracture," *Continuum Mechanics and Thermodynamics,* vol. 29, pp. 935-945, May 2015.

[25] J. Vignollet, S. May, R. de Borst and C. V. Verhoosel, "Phase-field models for brittle and cohesive fracture," *Meccanica,* vol. 49, pp. 2587-2601, January 2014.

[26] H. Ulmer, M. Hofacker and C. Miehe, "Phase-field Modeling of Fracture in Plates and Shells," *PAMM,* vol. 12, pp. 171-172, December 2012.

[27] S. Teichtmeister, D. Kienle, F. Aldakheel and M.-A. Keip, "Phase-field modeling of fracture in anisotropic brittle solids," *International Journal of Non-Linear Mechanics,* vol. 97, pp. 1-21, December 2017.

[28] M. Strobl and T. Seelig, "A novel treatment of crack boundary conditions in phase-field models of fracture," *PAMM,* vol. 15, pp. 155-156, October 2015.

[29] N. Singh, C. V. Verhoosel, R. de Borst and E. H. van Brummelen, "A fracture-controlled path-following technique for phase-field modeling of brittle fracture," *Finite Elements in Analysis and Design,* vol. 113, pp. 14-29, June 2016.

[30] P. Sicsic and J.-J. Marigo, "From Gradient Damage Laws to Griffith's Theory of Crack Propagation," *Journal of Elasticity,* vol. 113, pp. 55-74, October 2012.

[31] K. Seleš, T. Lesičar, Z. Tonković and J. Sorić, "A residual control staggered solution scheme for the phase-field modeling of brittle fracture," *Engineering Fracture Mechanics,* vol. 205, p. 370–386, January 2019.

[32] V. I. Sarrak, "BRITTLE FRACTURE OF METALS," *Soviet Physics Uspekhi,* vol. 2, pp. 150-164, January 1959.

[33] H. L. Ren, X. Y. Zhuang, C. Anitescu and T. Rabczuk, "An explicit phase-field method for brittle dynamic fracture," *Computers & Structures,* vol. 217, p. 45–56, June 2019.

[34] R. Rangarajan, M. M. Chiaramonte, M. J. Hunsweck, Y. Shen and A. J. Lew, "Simulating curvilinear crack propagation in two dimensions with universal meshes," *International Journal for Numerical Methods in Engineering,* vol. 102, pp. 632-670, August 2014.

[35] T. T. Nguyen, J. Réthoré and M.-C. Baietto, "Phase-field modelling of anisotropic crack propagation," *European Journal of Mechanics - A/Solids,* vol. 65, p. 279–288, September 2017.

[36] T. T. Nguyen, J. Yvonnet, M. Bornert, C. Chateau, K. Sab, R. Romani and R. Le Roy, "On the choice of parameters in the phase-field method for simulating crack initiation with experimental validation," *International Journal of Fracture,* vol. 197, pp. 213-226, February 2016.

[37] M. Negri, "Convergence analysis for a smeared crack approach in brittle fracture," *Interfaces and Free Boundaries,* pp. 307-330, 2007.

[38] M. Negri, "A finite element approximation of the Griffith?s model in fracture mechanics," *Numerische Mathematik,* vol. 95, pp. 653-687, October 2003.

[39] N. Moes, J. Dolbow and T. Belytschko, "A finite element method for crack growth without remeshing," *International Journal for Numerical Methods in Engineering,* vol. 46, pp. 131-150, September 1999.

[40] C. Miehe, E. Gürses and M. Birkle, "A computational framework of configurational-force-driven brittle fracture based on incremental energy minimization," *International Journal of Fracture,* vol. 145, pp. 245-259, October 2007.

[41] J.-J. Marigo and L. Truskinovsky, "Initiation and propagation of fracture in the models of Griffith and Barenblatt," *Continuum Mechanics and Thermodynamics,* vol. 16, pp. 391-409, May 2004.

[42] T. M. Maccagno and J. F. Knott, "The low temperature brittle fracture behaviour of steel in mixed modes I and II," *Engineering Fracture Mechanics,* vol. 38, pp. 111-128, January 1991.

[43] B. Li, C. Peco, D. Millán, I. Arias and M. Arroyo, "Phase-field modeling and simulation of fracture in brittle materials with strongly anisotropic surface energy," *International Journal for Numerical Methods in Engineering,* vol. 102, pp. 711-727, July 2014.

[44] D. Leguillon, "Strength or toughness? A criterion for crack onset at a notch," *European Journal of Mechanics - A/Solids,* vol. 21, pp. 61-72, January 2002.

[45] C. Kuhn and R. Müller, "Interpretation of parameters in phase-field models for fracture," *PAMM,* vol. 12, pp. 161-162, December 2012.

[46] P. Kasirajan, S. Bhattacharya, A. Rajagopal and J. N. Reddy, "Phase-field modeling of fracture in Quasi-Brittle materials using natural neighbor Galerkin method," *Computer Methods in Applied Mechanics and Engineering,* vol. 366, p. 113019, July 2020.

[47] A. Karma and A. E. Lobkovsky, "Unsteady Crack Motion and Branching in a Phase-Field Model of Brittle Fracture," *Physical Review Letters,* vol. 92, June 2004.

[48] V. Hakim and A. Karma, "Laws of crack motion and phase-field models of fracture," *Journal of the Mechanics and Physics of Solids,* vol. 57, pp. 342-368, February 2009.

[49] V. Hakim and A. Karma, "Crack Path Prediction in Anisotropic Brittle Materials," *Physical Review Letters,* vol. 95, December 2005.

[50] S. Goswami, C. Anitescu and T. Rabczuk, "Adaptive phase-field analysis with dual hierarchical meshes for brittle fracture," *Engineering Fracture Mechanics,* vol. 218, p. 106608, September 2019.

[51] A. Giacomini, "Size Effects on Quasi-Static Growth of Cracks," *SIAM Journal on Mathematical Analysis,* vol. 36, pp. 1887-1928, January 2005.

[52] G. A. Francfort, "Quasistatic brittle fracture seen as an energy minimizing movement," *GAMM-Mitteilungen,* vol. 29, pp. 172-191, October 2006.

[53] L. O. Eastgate, J. P. Sethna, M. Rauscher, T. Cretegny, C.-S. Chen and C. R. Myers, "Fracture in mode I using a conserved phase-field model," *Physical Review E,* vol. 65, February 2002.

[54] G. Del Piero, G. Lancioni and R. March, "A variational model for fracture mechanics: Numerical experiments," *Journal of the Mechanics and Physics of Solids,* vol. 55, pp. 2513-2537, December 2007.

[55] G. Dal Maso and R. Toader, "A Model for the Quasi-Static Growth of Brittle Fractures:Existence and Approximation Results," *Archive for Rational Mechanics and Analysis,* vol. 162, pp. 101-135, April 2002.

[56] J. D. Clayton and J. Knap, "A geometrically non-linear phase-field theory of brittle fracture," *International Journal of Fracture,* vol. 189, pp. 139-148, August 2014.

[57] L.-Q. Chen, "Phase-Field Models for Microstructure Evolution," *Annual Review of Materials Research,* vol. 32, pp. 113-140, August 2002.

[58] M. Charlotte, J. Laverne and J.-J. Marigo, "Initiation of cracks with cohesive force models: a variational approach," *European Journal of Mechanics - A/Solids,* vol. 25, pp. 649-669, July 2006.

[59] A. Chambolle, G. A. Francfort and J.-J. Marigo, "Revisiting Energy Release Rates in Brittle Fracture," *Journal of Non-linear Science,* vol. 20, pp. 395-424, April 2010.

[60] A. Chambolle, A. Giacomini and M. Ponsiglione, "Crack Initiation in Brittle Materials," *Archive for Rational Mechanics and Analysis,* vol. 188, pp. 309-349, November 2007.

[61] G. T. Camacho and M. Ortiz, "Computational modelling of impact damage in brittle materials," *International Journal of Solids and Structures,* vol. 33, pp. 2899-2938, August 1996.

[62] G. Caginalp and P. Fife, "Phase-field methods for interfacial boundaries," *Physical Review B,* vol. 33, pp. 7792-7794, June 1986.

[63] M. Buliga, "Energy Minimizing Brittle Crack Propagation," *Journal of Elasticity,* vol. 52, pp. 201-238, 1998.

[64] B. Bourdin, "Numerical implementation of the variational formulation for quasi-static brittle fracture," *Interfaces and Free Boundaries,* pp. 411-430, 2007.

[65] G. I. Barenblatt, "The formation of equilibrium cracks during brittle fracture. General ideas and hypotheses. Axially-symmetric cracks," *Journal of Applied Mathematics and Mechanics,* vol. 23, pp. 622-636, January 1959.

[66] I. S. Aranson, V. A. Kalatsky and V. M. Vinokur, "Continuum Field Description of Crack Propagation," *Physical Review Letters,* vol. 85, pp. 118-121, July 2000.

[67] L. Ambrosio, "Existence theory for a new class of variational problems," *Archive for Rational Mechanics and Analysis,* vol. 111, pp. 291-322, 1990.

APPENDIX A: ALGORITHM FOR MATLAB CODE

Step 1: Define Variables

Step 2: Define initial PDE parameters

Step 3: Create PDE models for Elastic problem and Phase-field crack problem

Step 4: Create 2D geometry with DECSG function with a rectangle and subtracting notches from it

Step 5: Append the final geometry to both PDE models after making a geometry model out of it

Step 6: Generate linear triangular mesh out of PDE models

Step 7: Apply Boundary conditions on the Top and bottom edges as displacement u, which grows with the increment delta with each iteration of steps

Step 8: Is Step = 0?

Step 8a: If yes, VT =1, and elastic energy and max elastic energy = 0

Step 8b: If no, Max elastic energy = elastic energy

Step 9: Define Elastic problem parameters using the value VT

Step 10: Solve elastic problem with elliptic PDE solver to determine Elastic energy after displacement

Step 11: For irreversibility condition,

Step 11a: if value of VT is less than 0.005 for any mesh element, elastic energy = max elastic energy for that element

Step 11b: Else, continue

Step 12: Define Phase-field crack problem parameters using the value of elastic energy

Step 13: The Phase-field crack PDE model is solved for the value of VT

Step 14: Check if the step is equal to total steps

Step 14a: If no, do step + 1 and go to Step 7

Step 14b: If yes, continue

Step 15: Perform post processing on the PDE model by adding contours for u and v and adding labels

Step 16: Display the final PDE plots for u and v

Step 17: End

APPENDIX B: MATLAB CODE

```
clear all;
close all;
%Parameters
Totalstep = 10;     % Total steps of the simulation
DeltaT = 0.1;       % Time interval
%Antiplane Elasticity parameters
Mu = 10;            % Shear Modulus
%%%%%%%%
a1 = 0.0;           % a assign a proper value
f1 = 0.0;           % f assign a proper value
%phase-field crack parameters
VT = 1;             % initializing crack phase-field parameter v
kappa = 0.04;       % Regularization parameter
%%%%%%%%
c2 = 2*kappa;           % c assign a proper value
f2 = 0.5/kappa;         % f assign a proper value
%% Create the PDE Model with a single dependent variable (Antiplane
displacement u)
numberOfPDE = 1;
pdem1 = createpde(numberOfPDE);
%% Create the PDE Model with a single dependent variable (Phase-field
parameter v)
numberOfPDE = 1;
pdem2 = createpde(numberOfPDE);
%% Geometry and Mesh
% Rectangle with two notches
width = 2;        % Width of rectangle
height = 2;       % Length of rectangle
LNotchL = 0.2;    % Length of notch left
LNotchH = 0.05;   % Half width of notch left
RNotchL = 0.2;    % Length of notch right
RNotchH = 0.05;   % Half width of notch right
lftloc = height*0.2;  % Left position of notch value from 0 to 1
rgtloc = height*0.8;  % Right position of notch value from 0 to 1
% define the geometry by giving the 4 x-locations followed by the 4
y-location.
gdm1(:,1) = [3 4 0 width width 0 height height 0  0]';
gdm1(:,2) = [2 3 0 LNotchL 0 lftloc-LNotchH lftloc lftloc+LNotchH 0
0]';
gdm1(:,3) = [2 3 width width-RNotchL width rgtloc+RNotchH  rgtloc
rgtloc-RNotchH 0 0]';
ns1 = char('R1', 'P1', 'P2');
ns1 = ns1';
g  = decsg(gdm1, 'R1 - P1 - P2',ns1);  % Subtracting the notches from
the rectangle
% Convert the DECSG geometry into a geometry object
% on doing so it is appended to the PDEModel
%%% Assigning the geomtry to the elastic problem (pdm1)
geometryFromEdges(pdem1,g);
%%% Assigning the geomtry to the crack phase-field problem (pdm2)
geometryFromEdges(pdem2,g);
% Plot the geometry and display the edge labels for use in the
boundary
figure;
pdegplot(pdem1, 'edgeLabels', 'off');
axis equal;
%title 'Geometry With Edge Labels Displayed';
title(sprintf('Geometry \n'));
```

```
xlabel 'X-coordinate (cm)'
ylabel 'Y-coordinate (cm)'
%% Create the mesh
% Create the triangular mesh on the geomtry
hmax = 0.01;      % element size
%Elastic problem
msh=generateMesh(pdem1,'Hmax', hmax, 'GeometricOrder', 'linear');
%phase-field problem
msh=generateMesh(pdem2,'Hmax', hmax, 'GeometricOrder', 'linear');
p=msh.Nodes;      % Number of nodes
t=msh.Elements;   % Number of elements
%%%%%%%%%%%%%%%
figure;
pdeplot(pdem1);
axis equal;
%%%%%%%%%%%%%%%%%%%%%%%%%%%%%%%%%%%%%%%%%%%%%%%%%%%%%%%%%%%%%%%%

for step=0:Totalstep
    time = DeltaT * step;     % Time
    ucTop = applyBoundaryCondition(pdem1,'Edge',1, 'u', time);
    ucBottom = applyBoundaryCondition(pdem1,'Edge',2, 'u', 0);

    if(step == 0)
        VT = 1;
        MaxElasticEnergy = zeros(1,length(t));
        ElasticEnergy = zeros(1,length(t));
    else
        MaxElasticEnergy = ElasticEnergy;
    end
    %%
    c1 = vt.^2*Mu;           % c1 assign a proper value
    %
    %% Solving
    % Elastic problem
    % The eliptic solver
    u(:,step+1) = assempde(pdem1,c1,a1,f1);
    [dudx,dudy] = pdegrad(p,t,u(:,step+1));
    area=pdetrg(p,t);
    % Calculating the elastic energy 0.5*Mu*|Du|^2
    ElasticEnergy = 0.5*Mu*(dudx.*dudx + dudy.*dudy);
    un = pdeprtni(p,t,ElasticEnergy);
    % irreversibility condition
    if(step > 0)
       for i=1:length(t)
           if(VT(i)<0.005)
             ElasticEnergy(i) = MaxElasticEnergy(i);
           end
       end
    end
    %%
    a2 = 2*(ElasticEnergy + 0.25/kappa); % a2   assign a proper value
    %
    %% Solving
    % Phase-field crack problem
    % The eliptic solver
    v(:,step+1) = assempde(pdem2,c2,a2,f2);
    % interpolating the nodal values on the elements
    VT = pdeintrp(p,t,v(:,step + 1));
end
figure;
```

```
pdeplot(pdem2, 'xydata', u(:,step), 'contour', 'off', 'colormap',
'jet');
title(sprintf('Distribution of Displacement u \n'));
xlabel 'X-coordinate (cm)'
ylabel 'Y-coordinate (cm)'
axis equal;
%%
figure;
pdeplot(pdem2, 'xydata', v(:,step), 'contour', 'off', 'colormap',
'jet');
title(sprintf('Distribution of the phase-field parameter v \n'));
xlabel 'X-coordinate (cm)'
ylabel 'Y-coordinate (cm)'
axis equal;
```

Geometry code for sample problem 2:

```
width = 1;               % Width of rectangle
height = 1;              % Length of rectangle
LNotchL = 0.5;           % Length of notch left
LNotchH = 0.0005;        % Half width of notch left
lftloc = height*0.5;     % Left position of notch value from 0 to 1
% define the geometry by giving the 4 x-locations followed by the 4
y-location.
gdm1(:,1) = [3 4 0 width width 0 height height 0  0]';
gdm1(:,2) = [2 3 0 LNotchL 0 lftloc-LNotchH lftloc lftloc+LNotchH 0
0]';
ns1 = char('R1', 'P1');
ns1 = ns1';
g  = decsg(gdm1, 'R1 - P1',ns1);  % Subtracting the notch from the
rectangle
```

APPENDIX C: GUI INTERFACE

The GUI for the code was made to input the sample geometry, the mesh size for geometry, and then inputs to define the size and location of notches according to a value from 0 to 1 which will define the location relative to the length of the specimen. The user can then use geometry, mesh and solve buttons to perform the said tasks.

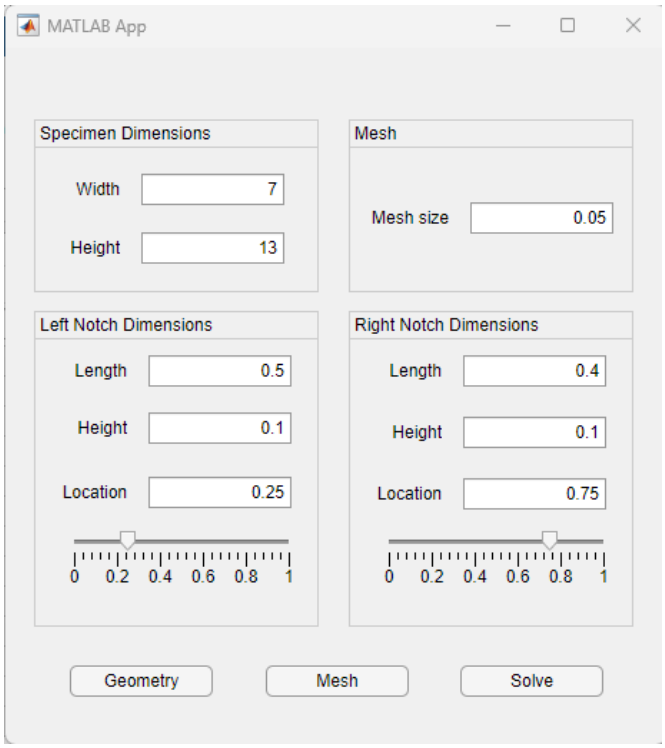

Figure C.1: GUI Interface

APPENDIX D: RESULTS

The second and third specimen simulation result had the expected S shaped crack propagation that is formed due to joining of crack tip from each notch. The crack propagation can be better understood by analyzing each step until the crack is observed. The phase-field parameter plot for each 10 steps until step 80 is analyzed to observe crack propagation in second test specimen 2. First, crack formation is seen on the tip of notch which gradually increases forwards until step 50 where phase-field parameter value decreases in the region between the two cracks that are forming. The phase-field parameter further decreases in the region and gets refined until it converges to a pattern of an S shape.

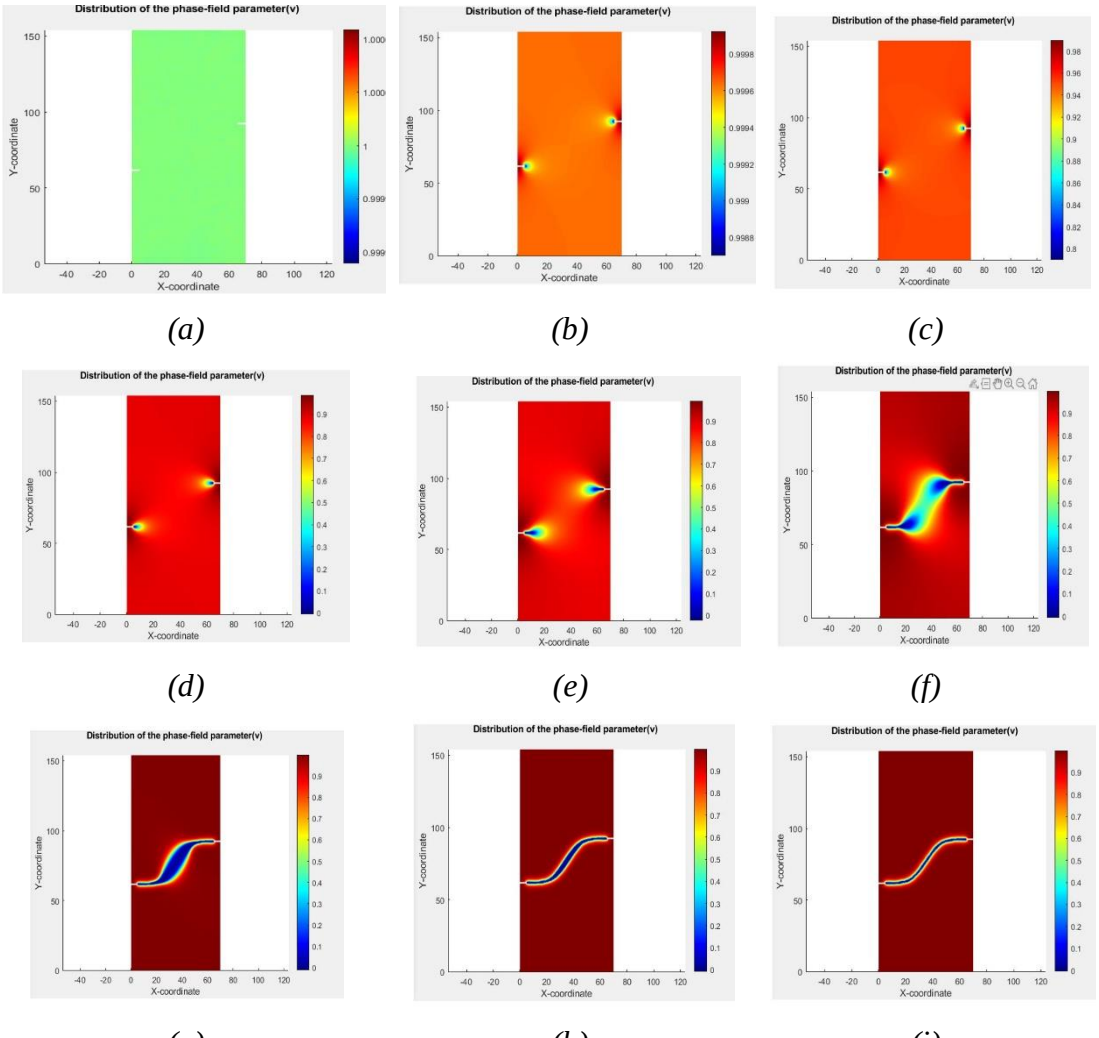

(a) *(b)* *(c)*

(d) *(e)* *(f)*

(g) *(h)* *(i)*

Figure D.1: Phase-field parameter distribution in test specimen 2 with time step increment of 10 upto 80

The video obtained from the recording throughout the experiment was also analyzed and a frame from each 6 seconds were taken. The frames showed a similar crack propagation pattern to that of simulation.

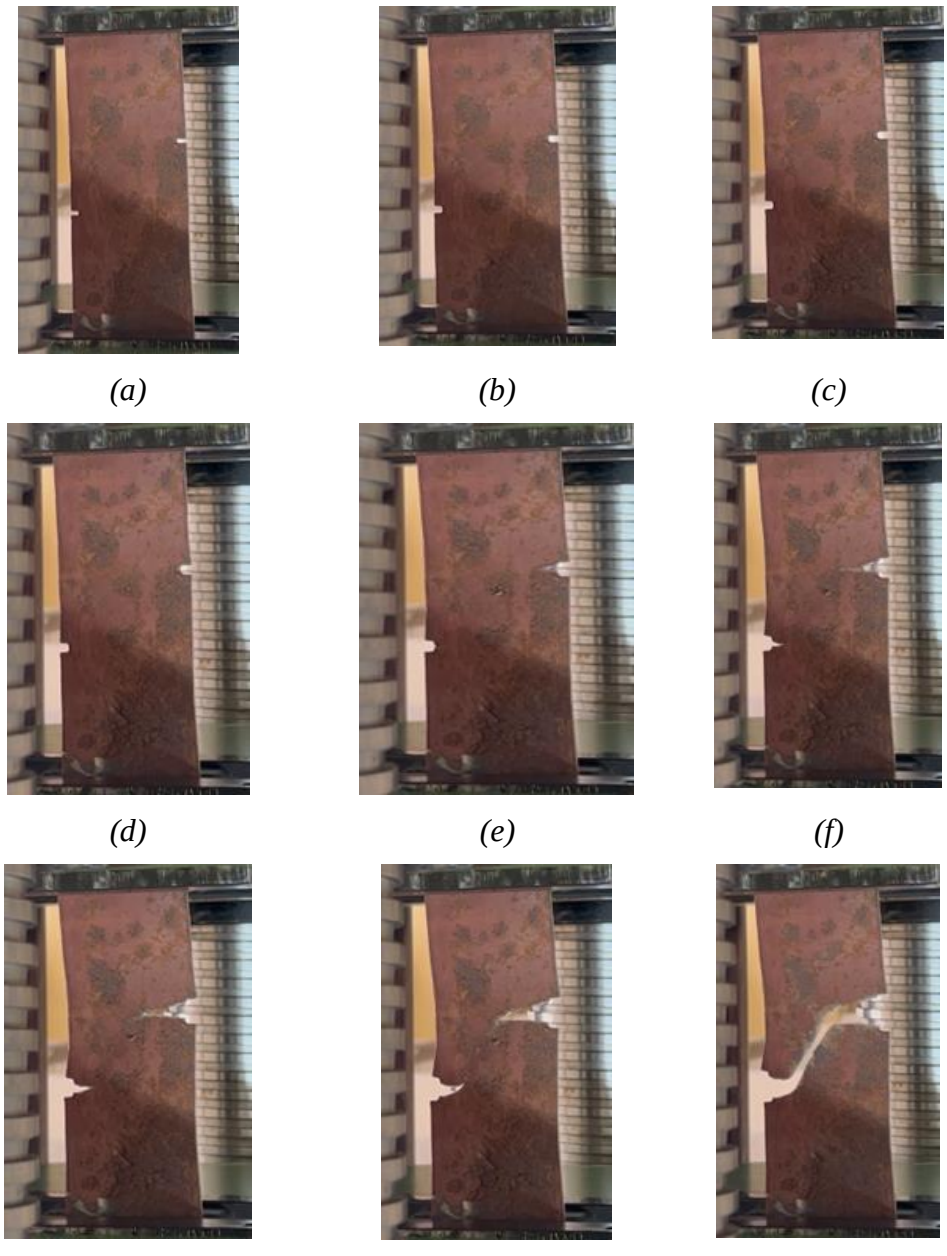

(a) *(b)* *(c)*

(d) *(e)* *(f)*

(g) *(h)* *(i)*

Figure D.2: Step by step timelapse of UTM testing in test specimen 3 in increment of 6 seconds